Driving Assistance for Optimal Trip Planning of Electric Vehicle Using Multi-objective Evolutionary Algorithms

M. Khanra, A. K. Nandi and W. Vaz

Abstract This chapter proposes a novel strategy (the so-called Driving Assistance system for Optimal Trip Planning, DAOTP) for electric vehicles (EV), which works based on a multi-objective optimization approach. DAOTP provides an optimal driving strategy (ODS) corresponding to minimum energy consumption, travel time, and discomfort. Since these objectives are conflicting with each other, a multi-objective optimization tool is adopted to solve the problem. Based on the current trip information, first a set of Pareto-optimal solutions (ODSs) is obtained, and then a preferred ODS is selected from them corresponding to a higher level information or using problem-specific multi-criterion aspects for implementation. DAOTP works using route information obtained through GPS (Global Positioning System), Internet, etc. Route information includes the road surface type, weather conditions, trip start and end points, etc. In this chapter, the DAOTP system architecture, concerned MOOP, and the related EV models are presented in details. A brief explanation of multi-objective genetic algorithm that solves the present MOOP is given. The operation of DAOTP is elaborately presented with an application in a simple urban micro-trip planning. After that, the application of DAOTP for highway and complex trip planning are presented. The DAOTP results found in high-speed driving cycles are analyzed. The effectiveness of DAOTP is presented considering some sample trips, and its results are analyzed with varied route characteristics and trip complexity.

Keywords Electric vehicle · Trip planning · Driving assistance
Multi-objective optimization · Evolutionary algorithm · Energy consumption
Trip time · Driving comfort

M. Khanra · A. K. Nandi (✉)
CSIR-Central Mechanical Engineering Research Institute (CSIR-CMERI), MG Avenue, Durgapur, West Bengal, India
e-mail: nandiarup@yahoo.com

W. Vaz
Department of Engineering, University of Wisconsin Colleges, UW-Fox Valley, Menasha, USA

S. Datta and J. P. Davim (eds.), *Optimization in Industry*, Management and Industrial Engineering, https://doi.org/10.1007/978-3-030-01641-8_7

1 Introduction

As the time passes, research efforts are bringing more and more improvements to the vehicular sector. These improvements are broadly classified into two categories. One involves the hardware of the vehicle. Other improvements, which belong to the Intelligent Transportation System domain, are for driver assistance. The primary goal is to ease the driving experience and properly manage available resources. Some aspects are automatic fixed-distance following navigation and route guidance, operational cost reduction, obstacle avoidance, maintaining the lane, parking assistance, improving comfort and safety, and so on. Some of the various strategies and initiatives that were adopted in the past are described as follows.

In the Automated Highway Systems (AHS), multiple vehicles are coupled electronically for controlling them automatically toward driving at the same speed and safe following distances [81, 91]. AHS forms a semi-autonomous platoon by controlling the vehicles longitudinally as well as tangentially [7]. In a semi-autonomous platoon, one vehicle (preferably which is in the front) is driven actively, and the other vehicles are followed automatically. Under the project KONVOI, funded by German's Federal Ministry of Economics and Technology, an Advanced Driver Assistance System (ADAS) was developed to automatically control the longitudinal and lateral movement of the vehicles behind the actively driven preceding vehicle [57]. ADAS includes six primary components: GPS (Global Positioning System) [41], UMTS (Universal Mobile Telecommunications System) for vehicle–infrastructure communication [91], DIS (Driver Information System) [93], AG (Automated Guidance) [75], WLAN (Wireless Local Area Network) for vehicle–vehicle communication [45], and ACC (Adaptive Cruise Control) [99]. All these modules are connected to a central server. Details of various AHS and ADAS forms and related undertaken projects can be found in [5]. Such systems are primarily suitable for traffic control and safety. AHS and ADAS do not focus on any direct energy management of the vehicle, and can be adopted irrespective of the vehicle type.

There are various navigation systems that help drivers by providing an eco-driving or eco-routing functionality. Vexia's ecoNav solution [94] assists the driver by proving the fuel consumption rate that is determined based on the characteristics of vehicle and driving behavior. Garmin's ecoRoute software [38] finds a fuel-efficient route on the basis of road information and vehicle characteristics. The Freightliner Predictive Cruise Control [86] minimizes the fuel consumption rate by fine-tuning the vehicle speed corresponding to the route driving cycle. Like AHS, the above navigation systems can be adopted irrespective of vehicle type.

Traditionally, routing has focused on exploring shortest paths in a network based on the costs of positive and static edges that represent the distance between two nodes. Contrary to other vehicles, solving routing problems for EV is a challenging work because of the negative edge cost due to regenerative braking, vehicle weight, and limited battery capacity (resulting in the cost of a path being no longer just the sum of its edge costs). Considering these challenges, an attempt was made in [30, 76] to find a solution for energy-optimal routing for EVs. Recently, a few industrial initiatives

were undertaken to deal with the routing issues of EV [13]. NAVTEQ ADAS [69] deals with finding routes that can minimize ICEV fuel consumption and EFV energy consumption by considering additional route information such as altitude, slopes, and curves.

A European Commission-sponsored research project called "Intelligent Dynamics for fully Electric Vehicles" (ID4EV) [77] was initiated to establish an intelligent system which is most energy-efficient and HMI (Human–Machine Interface) capability, and safe braking and chassis systems as well as intelligent functionalities and new Human–Machine Interface (HMI) concepts for the needs of EVs, as for such system it is important for FEVs to have wide acceptability [48]. Various aspects of ID4EV projects can be found in [106].

Another way of driving assistance is the adoption of cooperative driving (a type of AHS), where a flexible platooning is formed among the vehicles which are available within a short distance over a couple of lanes [53]. The cooperative driving technology is based on two studies: Super Smart Vehicle System (SSVS) [87] and inter-vehicle communications with infrared rays from [35]. This driving assistance is primarily focused on the compatibility of safety and efficiency of road traffic.

Similar to other vehicles, EVs possess an inadequate energy storage that results in a short driving range. Moreover, refueling of EV is time consuming due to the long charging time of the battery. In addition, inadequate battery charging stations in contrast to fueling stations of Internal Combustion Engine (ICE)-based vehicles is a critical issue for EVs. As a consequence, efficient usage of battery energy is crucial for EVs. On the other hand, that is not so important for ICE vehicles. Thus, in order to extend the EV range by minimizing energy consumptions, it is required to adopt an optimal driving strategy (ODS) during driving. Additionally, due to the above-stated shortcomings, an appropriate trip plan corresponding to the present battery state-of-charge (SOC) is required prior to the journey start. Many times, due to unanticipated circumstances, deviation from the previous trip plan is happening. The driver needs to deviate from the preplanned trip during the journey. In such conditions, an online assistance is helpful to the drivers toward replanning the rest of the journey. Various issues are required to consider during trip planning such as whether with the remaining battery charge can reach to destination or not [96], what driving strategy to be followed corresponding to the road type for comfortable journey and minimum battery charge depletion [40, 42] and shortest trip duration [60], and what extent the trip expenditure (e.g., cost of charging) can be reduced [82].

A driving strategy refers to the value(s) of all or any of the parameters, namely, speed, acceleration, acceleration duration, deceleration, and deceleration to be applied by the driver during running a vehicle. In order to maintain the above issues, drivers are required to assist during trip performing by suggesting the optimal driving strategy to be followed and corresponding EV range and trip end battery SOC to be expected. An optimal driving strategy can be determined by taking into consideration concurrently three conflicting objectives such as minimum energy consumption, minimum trip time, and maximum driving comfort.

In this regard, the above-stated driving assistance systems are useful but not sufficient for an EV to compete or become comparable to the other vehicle types. In addition to knowing that an EV is a zero emission vehicle and comparatively more efficient such a driving assistance for optimal trip planning is extremely necessary to instill more confidence in EV drivers and to increase the interest of the general public in EVs. From a psychological standpoint, a reliable trip plan with accurate range estimation provided to drivers may be more significant than actually increasing the range of an electric mobility system [34]. Realizing such motivation, researchers propose various new methods and intelligent strategies. For example, due to the limited battery capacity, the driver was assisted by providing a locality-based optimal charging station planning. In [32], the number of charging stations was estimated using a weighted Voronoi diagram compliant with a conventional standard charging station capacity. An optimum charging method was proposed in [84], which includes an individual charging plan for each vehicle while reducing the electricity cost, avoiding distribution grid congestion, and fulfilling the individual vehicle owner's necessities.

With the intention of increasing the EV energy efficiency and range autonomy, Demestichas et al. [25] introduce an autonomous route planning method based on advanced machine learning techniques which monitors the energy consumption continuously. An EV suitability ADAS was designed for traffic estimation and selection of optimal route in [25, 26] suitable for EVs was designed and implemented with traffic estimation and optimal route selection capabilities. It helps the driver to make an appropriate routing decision so as to energy saving and residual range enhancement.

In order to find the best route, a fleet management planning for EV was proposed in [63]. It considers energy consumption based on the road architecture, environmental conditions, vehicle characteristics, driving behavior, traffic situations, and locations of electric charging stations. An advanced EV fleet management architecture was presented in [63], where the best route was decided based on electric power consumption considering information about the road topology (elevation variations, source, destination, etc.), weather conditions, vehicle characteristics, driver profile, traffic conditions, and electric charging station locations. A generalized multi-commodity network flow (GMCNF) model analogous to space exploration logistics [50] was proposed in [17] for finding the best route on the basis of energy consumption and battery charging time.

However, from the previous studies in the literature, it was found that majority of driving assistance systems deal with energy consumption. In most of the systems, energy consumption and trip time are treated separately, and a correlation between them was tried to establish [27]. An energy-driven and context-aware route planning framework for EV is found in [95]. An optimal route is decided here by minimizing the cost function which comprises the trip time and energy consumption. However, there is no such driving assisting systems that consider energy consumption, trip time, and driving comfort simultaneously. In [28], the authors made an attempt to find a driving strategy for ICE vehicles by simultaneous consideration of total travel time, and fuel consumption, and driving discomfort. Indeed, consideration of these three factors is important. The present chapter explores the need for and the requirements of

considering these three aspects simultaneously for optimal trip planning. It describes the related problem and a possible way of implementing in practical application for an EV. A novel framework, Driving Assistance for Optimal Trip Planning (DAOTP), is proposed to guide the driver for trip planning and to drive the EV in an efficient manner. The framework of DAOTP is context-aware as well as energy-efficient since it incorporates real-time traffic and route data, and accounts for multiple driving aspects including trip time, comfort driving, and energy efficiency.

The present DAOTP system first finds a set of Pareto-optimal solutions (ODSs) to the driver after solving a multi-objective optimization problem based on the current route and environmental data. The trip end battery SOC and total trip time corresponding to those optimal driving strategies for a specified trip length are also shown.

A preferred ODS is selected from them corresponding to a higher level information or using problem-specific multi-criterion aspects for implementation.

2 Proposed System of Driving Assistance for Optimal Trip Planning (DAOTP) for an EV

An EV driving assistance system is proposed here. The system presents a number of optimal driving strategies to the driver along with the corresponding driving range, trip end SOC, and total trip time [52]. It works based on a multi-objective concept, where multiple conflicting objectives are considered simultaneously to fix the optimal decision variable(s). Figure 1 demonstrates the architecture of DAOTP system. The system consists of two modules namely HMI (Human–machine interface) and DAOTP. HMI is used to interface between the driver and the DAOTP system with the help of GPS/Internet or other media.

DAOTP assists the driver by endowing with the following information regarding ODS at the time of executing and prior to a trip.

1. Reference acceleration(s)/deceleration(s)
2. Reference trip speed
3. Predicted range corresponding to the present battery SOC
4. Predicted Battery SOC and time at trip completion

The EV trip has three modes: acceleration, constant speed, and deceleration. DAOTP system deals with the first two zones. Since during deceleration, there is a gain of energy through the regenerative system finding an optimal driving strategy for deceleration is not considered here. There is an availability of many studies [15, 16, 100] suggesting how to regenerate maximum energy during deceleration of an EV. Such strategies can be easily incorporated into DAOTP system. In the present study, the electric motor brakes the EV at a constant rate that has a weak dependence on the vehicle speed. In order to estimate trip time prior to the trip, it was required to pick a constant deceleration value for different speed zones.

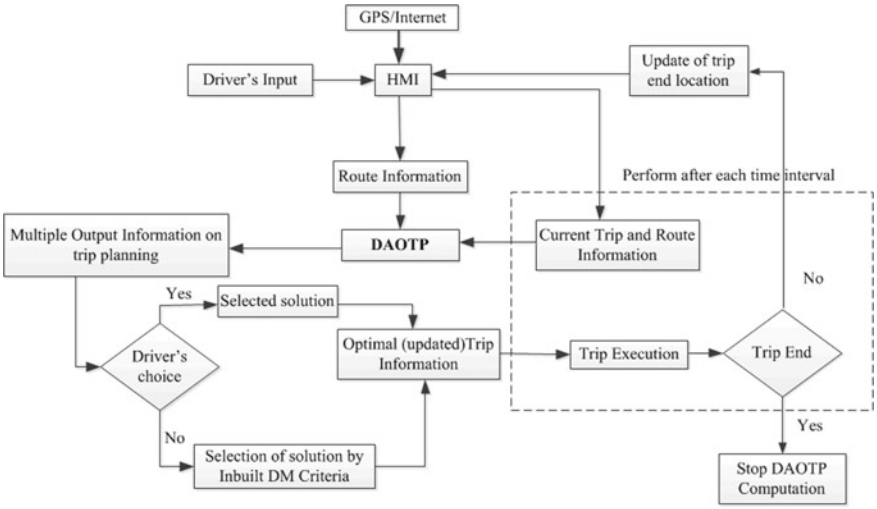

Fig. 1 Schematic layout of DAOTP system architecture

2.1 Working Methodology of DAOTP System

According to the driver's trip start and end locations, the HMI in association with GPS and Internet finds different routes if they exist. The HMI can be attached to the dashboard or mobile through a wireless link like a smartphone. Unless there is a specific choice by the driver, an optimum route is generally selected based on less number of stops, short route distance, good road conditions, less traffic at the time of journey, etc., and such information may be obtained based on past statistical data of route traffic and present traffic conditions. There are separate transportation studies (scheduling and routing problems) [10] that consider how to select an optimal route corresponding to multiple stops, time scheduling, multiple vehicles, etc. The present chapter does not include such optimization problems. The objective of the proposed DAOTP is different from that of scheduling and routing problems. Once a route is specified, DAOTP receives various route data through GPS and/or other resources using HMI. Additionally, the system receives the current battery SOC, EV auxiliary load, etc., with the help of appropriate measuring devices [73] and data acquisition system. Execution of DAOTP is carried out by solving the associated MOOP based on the received data for the chosen route. Once the DATOP execution is completed, a set of solutions (ODS) and corresponding various predicted information (such as range, trip end SOC, and trip time) is presented to the driver for making a suitable trip planning. The driver may choose an appropriate ODS from the solution set based on the present circumstances or his desire. Otherwise, any decision-making technique may be adapted to select a preferred one. The driver is recommended to follow the preferred ODS for driving to the further ODS as evaluated in the subsequent DAOTP execution. The subsequent execution of DAOTP is performed on the basis

of current route data corresponding to the original or updated trip start/end location (destination) and battery SOC.

Various higher level information may be considered by driver for making a decision to choose a preferred solution, such as remaining trip length, trip time, road condition(s), speed limit(s), traffic clogging, etc. Prior knowledge of the range and total trip time for multiple ODSs provides enough flexibility to the drivers to adopt a most suitable ODS that consumes minimum energy resulting in a better range. It is particularly beneficial in a circumstance of low battery change where the driver wants to get to a charging station. Therefore, the key motivation behind DAOTP development is to predict the EV range and trip time for optimal speeds.

During the running of the EV, DAOTP collects various data from different sources after a certain time step. It does so repeatedly considering that trip conditions may change quickly and unpredictably. Based on these updated data, DAOTP executes again and presents a new set of solutions for the rest of the trip. If there are no considerable changes, these solutions would be almost identical to that suggested in the previous time step. That new solutions assist the driver to drive the vehicle accordingly so that he/she can complete the entire trip in an efficient manner while accounting for continuously changing trip conditions. This online functionality of DAOTP accounts for any unanticipated driving circumstances and any variation from the current ODS.

Various inputs to be provided by the driver to DAOTP are as follows:

- Immediate destination.
- Either select a route after getting a feedback from GPS for different possible routes depending on his/her choice or allow the system to choose the route having a shorter distance, less traffic congestion, and fewer stops.
- Maximum allowable trip time.
- Information on auxiliary energy consumption.

  It may be noted that certain data, such as auxiliary energy consumption, are relayed directly to DAOTP and do not require active input from the driver. The driver may choose to increase or decrease the auxiliary energy consumption before DAOTP, like switching the air conditioning off, in order to see what effect it has on the solutions, and he/she may increase or decrease the auxiliary energy consumption during the trip.

  Various step-by-step roles of HMI through GPS/Internet in DAOTP are presented as follows:
- Identify the present location of EV, and then suggests different possible routes to reach the destination.
- Calculate the number of stops in the entire trip for the chosen route and other related route information such as trip distance, traffic congestion, weather condition (wind velocity and direction, rainfall or others), and road conditions (road gradient and quality).
- Based on route information, divide the entire trip into smaller “micro-trips”. Identify different parts of each micro-trip based on the upper and lower speed limits associated with each part. The upper and lower speed limits already take into con-

sideration the road type and profile (e.g., sharp bending, steep gradient, etc.). The magnitude of upper and lower speed limits can be used to define the driving cycle type.

For ease of understanding, the working method of DAOTP is described for a micro-trip. The range and trip time calculations on a trip are described in Sect. 5.

3 Micro-trip and Route Characteristics

A micro-trip may be defined as an excursion between two successive locations of travel route at which the vehicle is definitely stopped [3, 44]. In general, an entire trip comprises several micro-trips. The length (range) of a micro-trip is defined by the distance covered the two stop points of vehicle, and may be called the start and end points of that micro-trip, respectively. A typical micro-trip consists of the following modes or phases:

(i) *Initial acceleration phase*—acceleration(s) to change speed from $v_{\text{ref\_previous\_trip}}$ (end reference speed of the previous micro-trip) to $v_{\text{ref1\_micro - trip}}$ (reference speed of the current (first part) micro-trip) if $v_{\text{ref\_previous\_trip}} < v_{\text{ref\_micro - trip}}$.

(ii) *Constant speed change*—keep running with $v_{\text{ref\_micro - trip}}$, which must be within the speed limit.

(iii) *Speed limit change*—if there is a change in the speed limit during the micro-trip (in case of multiple parts, as shown in Fig. 2), then deceleration(s) to change speed from $v_{\text{ref1\_micro - trip}}$ (reference speed of the first micro-trip part) to $v_{\text{ref2\_micro - trip}}$ (reference speed of the second micro-trip part) before the vehicle reaches the new speed limit zone if $v_{\text{ref2\_micro - trip}} < v_{\text{ref1\_micro - trip}}$, and continue to drive vehicle at $v_{\text{ref2\_micro - trip}}$ during the speed limit zone or acceleration(s) to change speed from $v_{\text{ref1\_micro - trip}}$ to $v_{\text{ref2\_micro - trip}}$ after the vehicle reaches the new speed limit zone if $v_{\text{ref2\_micro - trip}} > v_{\text{ref1\_micro - trip}}$.

(iv) *Final deceleration phase*—deceleration from $v_{\text{ref2\_micro - trip}}$ (reference speed of the current (end part) micro-trip) to $v_{\text{ref\_next trip}}$ (reference speed at the starting of next micro-trip) if $v_{\text{ref\_micro - trip}} > v_{\text{ref\_next\_trip}}$.

According to safety and differentiation of the type of trip, micro-trip comprises one or multiple types of road. Based on the lower and upper speed limits, roads are classified into four different types [8, 74] namely neighborhood (8–40 km/h), urban (40–56 km/h), highway (56–88.5 km/h), and interstate (88.5–112.6 km/h). The minimum and maximum speed limits of each driving cycle need to be strictly followed by the driver. Thus, the proposed DAOTP system must provide valid solutions for each driving cycle. Accordingly, its performance for each driving cycle was studied independently.

Figure 2 demonstrates the velocity profile of a typical complex micro-trip that consists of three parts. The first and third parts of the micro-trip correspond to a low-speed driving cycle and the second part corresponds to a high-speed driving cycle.

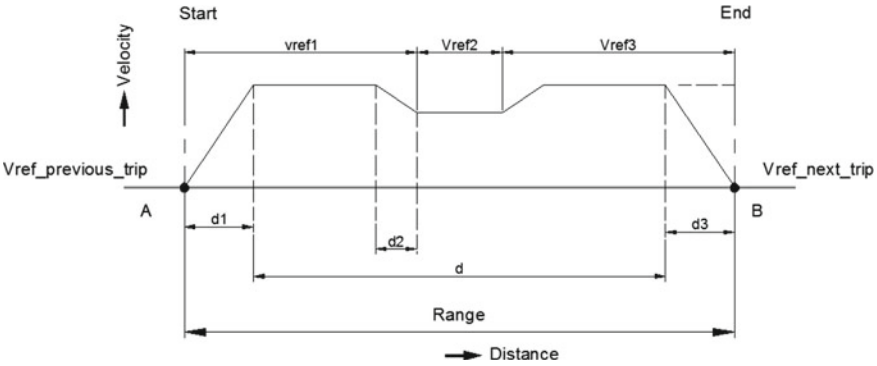

Fig. 2 Velocity versus distance plot of a typical micro-trip

The vehicle reference speeds, $v_{\text{ref1\_micro - trip}}$ and $v_{\text{ref3\_micro - trip}}$, belong to first and third parts of the micro-trip, respectively, whereas $v_{\text{ref2\_micro - trip}}$ is the reference speed associated with the part of the micro-trip. According to the definition of a micro-trip, $v_{\text{ref\_previous\_trip}}$ and $v_{\text{ref\_next trip}}$ in Fig. 2 are zero. According to the rule of traffic lights, at each light, the vehicle has to stop at a red signal light until the signal becomes green. Points A and B (in Fig. 2) are considered as two successive red signals. They could also represent a stop sign. Besides the driving strategy characteristics (DSC) such as speed, acceleration(s), and the respective durations, other environmental and physical factors (information that may be gleaned through various HMI inputs) associated with micro-trip route are the route characteristic parameters (such as road gradient, quality of road surface, air density, wind velocity and its direction, etc.), passenger weight, auxiliary load, start and end location of the micro-trip, road speed limits, initial SOC, etc. The route characteristic parameters are normally defined based on the distance covered and can be obtained through GPS or Internet sources. The other parameters are case-based depending on the driver's desire. For example, a road gradient varies with road length. To determine its value at a particular location on the road, one has to refer to how much distance is covered by the vehicle from a reference point, in general, the start point of micro-trip. Other parameters are dependent on the driver's desires. For example, the driver decides when the air conditioning is running and when it is not.

4 Control System

The control system is the interconnection of components that gives the desired output. Driving a car with the desired speed is the example of closed-loop control system. Here the system (presented in Fig. 3) compares the speed of the car with the desired speed. If any deviation in speed from desired speed, then the controller may increase or decrease the speed so that the deviation becomes zero. The sensor is used to

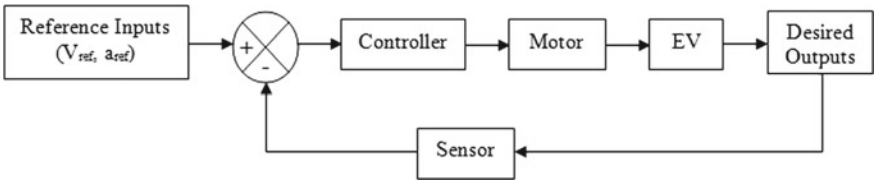

Fig. 3 Basic block diagram of EV speed control system

measure the controlled variables of the system and fed to the input. Then the control system compares the reference inputs (speed/acceleration) with a present output, which is fed by the sensor from the output.

The PI (proportional and integral) controller is used to control the EV acceleration and also maintains a constant speed of EV. The PI controller works during acceleration of EV for changing the speed and when the desired speed is reached, the integral action is switched off. Then only proportional action is activated and maintains a constant speed. The reference speed (v_{ref}) and the reference acceleration (a_{ref}) are used as the input of the controller. The output speed (v) and acceleration (a) are fed back to the input of controller in opposite phase to get desired output and stabilize the system.

5 Range and Trip Time Calculation

As mentioned previously, knowing the range, trip time, and final SOC value is essential for the driver to properly plan a trip. Existing methods for range calculation are summarized as follows. Battery State-of-Charge methods primarily concentrate on precisely calculating the battery SOC (which is similar to the fuel gage on a ICE vehicle) so as to find an estimation of how much battery charge remains. The range to be completed by the residual battery energy can be approximately determined based on the previous knowledge of what distance was covered by depleting how much battery charge. Various studies on battery SOC method based range estimation [6, 14, 29, 46, 80, 83, 85, 101] are found in the literature. This information, while important, is inadequate by itself since the battery's residual energy can be utilized in many different ways according to the driver's preferences. However, it should be optimally utilized to accomplish the driver's purpose. No such appropriate driving strategy is available to the driver to properly utilize the residual battery energy. In addition, since road conditions may vary in course of trip performing, the existing methods are unable to capture such changeable effects as they are intrinsically averaging methods. Energy-based methods calculate the energy utilization based on the current or recent trip and vehicle data Based on the amount of energy consumption rate, the EV range is predicted for the remaining battery charge. An approach to predict the residual driving range and driving time of ICE vehicles using Artificial

Neural Network (ANN) was found in [20]. In that approach, fuel capacity (remaining fuel), engine speed, vehicle velocity and weight, and road slope were considered as the inputs. Though this approach offers valuable information in the course of trip performing based on instantaneous driving parameters, the anticipated range is not known to the driver prior to trip started. Moreover, that approach does not suggest any optimum trip parameters. In [79], an ANN based technique was proposed to calculate the energy utilization for both pure and plug-in hybrid EVs in real-world driving situation. This technique considered various inputs such as average speed, average acceleration, total distance traveled, total duration, etc., to envisage the road category and traffic congestion and, finally the predicted EV energy consumption rate was found to deviate from the measured value y in the range of 20–30 to 70–80%. The authors recommend that as the energy consumption rate and total available energy are known, an accurate EV range prediction can be made using this technique. Once more, the driver does not have knowledge of the anticipated range for the specified conditions stated in the article to devise a driving strategy. An approach to envisage the power for the instant future requirement in EV was proposed in [54]. This approach considers the data from previous power consumption history, acceleration and speed, and road information obtained from a pre-downloaded map. Though the primary motivation of this study was the safety of battery, value of immediate power requirement could be used to calculate the range as well. But this approach is a passive method as the power requirement prediction depends on the driver's actions, and it does not suggest how to formulate a driving strategy.

There are three driving modes in which a vehicle can travel a distance. Two are during the vehicle's acceleration and deceleration and the other is when the vehicle is running at a constant speed. The methodology of finding the estimated distance traveled by a vehicle in these driving modes is presented in the following.

The range (distance) that can be traveled by an EV during constant speed mode is

$$R_g = v_{ref} \times T_v \tag{1}$$

where v_{ref} is the (uniform) speed at which the vehicle is moving and T_v is the corresponding duration. But, in practice, it is very difficult to maintain the vehicle's real speed exactly at v_{ref}, always. Thus v_{ref} is also considered as the commanded/desired speed. Once the accelerator is pressed and its position maintained, it takes some time (acceleration period) for the real vehicle speed, v, to get to v_{ref}. Thus, the instantaneous speed error is calculated as

$$e_v = v_{ref} - v \tag{2}$$

In steady state, v_{ref} and v are close enough to be considered equal from a vehicular standpoint. These two parameters were inputs to the speed controller. Now to cover an R_g with less stored battery energy consumption per unit time, the value v_{ref} becomes low. But, it results in a high T to obtain the same range. On the other hand, a decrease of T means consuming more energy. Thus to find an optimal v_{ref} to cover R_g efficiently,

two contradictory objectives namely minimization of total energy consumption and driving time are required to be solved simultaneously [89].

On the other hand, the range that can be covered by an EV during acceleration is

$$R_g = v_{init} T_a + \frac{1}{2} a_{ref} \times T_a^2 \tag{3}$$

where a_{ref} is the (uniform) acceleration (also called commanded or desired acceleration) at which the vehicle speed increasing to v_{ref} and T_a is the driving time during which a_{ref} can be plausibly retained by the battery. The instantaneous acceleration error is defined as the difference between the commanded acceleration and the real vehicle acceleration, a

$$f = a_{ref} - a \tag{4}$$

Both a_{ref} and a were inputs to the acceleration controller. Like optimal velocity, to find optimal acceleration(s), both the acceleration time and energy consumed for the acceleration are required to be minimized concurrently [68], and after solving such MOOP, it was revealed that a better optimization result is noticed using multiple accelerations compared to a single acceleration. Such analogous results were also observed in [49, 62]. Besides the above objectives, it is necessary to have sufficient comfort during driving. A discomfort journey may result in various health problems [42].

The range covered by an EV during deceleration is

$$R_g = v_{ref} T_d - \frac{1}{2} a_{dec} \times T_d^2. \tag{5}$$

where T_d is the duration for v_{ref} to reach a termination value (normally a low value, say 1 m/s). The EV deceleration was controlled by the speed controller rather than the acceleration controller.

In practice, a trip consists of several such driving modes. The total range (R) overcome by an EV in a typical trip is the summation of all R_g in these three driving modes and the total trip time is the summation of all corresponding T. In order to maximize the EV range and minimize the trip time by means of efficiently using the stored battery energy, the primary concern is to identify the optimal values of v_{ref}, a_{ref}, and a_{dec}. Various extraneous driving-specific parameters that affect v_{ref}, a_{ref}, and a_{dec} can be categorized into three groups: dynamic parameters, static parameters, and navigation control parameters [106]. For the sake of simplicity and reducing the model complexity, inherent model-specific parameters such as driveline dynamics, etc., were not considered, whereas route specific parameters that tend to change during a trip (gradient, elevation, wind, and road surface) were considered in this study. Neglecting these latter parameters can lead to large error in the results due to their more significant contribution to the overall energy consumption [40, 59, 97, 103].

6 Multi-objective Optimization

Optimization is one of the most frequent and persistent problems in real-world systems including engineering. Through this technique, one can reach to an extreme solution corresponding to either maximum or minimum of any objective subject to certain constraints. Contrary to single objective optimization, MOO plays an important role in decision-making toward making a preference among several options related to multiple contradictory objectives. Multiple contradictory objectives are normally found in most of the real-world problems. If all objectives are equally important, extreme value principle (as used in single objective optimization) cannot be adopted to arrive a solution. In such case, a number of solutions may be created based on a negotiation among the objectives. Such negotiation does not allow to consider a solution that is optimal corresponding to simply one objective. Thus, it is required to obtain a set of solutions, among them the designer is allowed to choose one that will fulfill the original intention. Selection of a solution among multiple availabilities is also known as multiple criterion decision-making (MCDM). Thus, the primary motivation for solving truly MOOPs is to find a set of non-dominated solutions. The front formed by the optimal non-dominated solutions is called Pareto-optimal front. The Pareto-front is formed by the solutions in which any change in any of the decision variables aimed at improving a particular performance index will produce deterioration in some of the other performance indices.

In general, a multi-objective problem (MOP) comprises of n number of input parameters (called decision variables, $x_{1,\ldots,n}$), k number of objective functions ($y_{1,\ldots,k}$), m inequality constraints, and j equality constraint. Objective functions and constraints are functions of the decision variables. The optimization goal is as follows:

$$\text{Maximize/minimize} \quad y = f\left(x_{1,\ldots,n}\right) = \left(f_2\left(x_{1,\ldots,n}\right), f_1\left(x_{1,\ldots,n}\right), \ldots, f_k\left(x_{1,\ldots,n}\right)\right) \tag{6}$$

$$\begin{aligned} \text{subject to} \quad & e\left(x_{1,\ldots,n}\right) = \left(e_1\left(x_{1,\ldots,n}\right), e_1\left(x_{1,\ldots,n}\right), \ldots, e_m\left(x_{1,\ldots,n}\right)\right) \leq 0, \\ & h\left(x_{1,\ldots,n}\right) = \left(h_1\left(x_{1,\ldots,n}\right), h_1\left(x_{1,\ldots,n}\right), \ldots, h_j\left(x_{1,\ldots,n}\right)\right) = 0, \end{aligned}$$

$$\begin{aligned} \text{where} \quad & x_1, x_2, \ldots, x_n \in X \\ & y = (y_1, y_2, \ldots, y_k) \in Y \\ & x_i^L \leq x_i \leq x_i^U, \quad i = 1, 2, \ldots, n \end{aligned}$$

The decision space and objective space are denoted by X and Y, respectively. x_i^L and x_i^U are the lower and upper bounds of each decision variable, x_i which form X. The feasible solutions must satisfy the variable's upper and lower limits and the constraints, $e(x)$ and $h(x)$.

Even though it is sufficient to know the objective ranges and Pareto-optimal shape in order to make a decision, it is essential to select a distinct preferred solution since it will be ultimately used for execution in a driving condition, and the corresponding task is very crucial. According to the categorization made by Veldhuizen and Lamont [92], the articulation of preferences may be carried out either before (a priori) or after (a posteriori) or during (progressive) the optimization search. In this work, two a posteriori-based MCDM techniques were adopted. Reference point based technique [64] identifies a preferred solution based on a reference point. Whereas in the second technique, first a knee-zone [11] on the Pareto-front is identified on the basis of trade-off among the objectives, then based on the higher level information, a preferred solution is selected from the knee-zone.

Various characteristics relating to the problem domain may be considered to decide the reference point. Ideal point is widely used as a reference point in many multi-objective problems. The set of optimal values obtained through optimization process considering each objective independently is referred to the ideal point which is considered here as a reference point in decision-making process. In the present work, a preferred solution among the Pareto-optimal set is identified on the basis of the minimum (Euclidean) distance from the reference point. Sometimes it is noticed that there is a typical portion of the Pareto-optimal front where a small improvement in one objective would lead to a large deterioration in any of the other objectives is treated as the knee-zone. The knee-value of the ith solution in the knee-zone is mathematically defined by Eq. (7) for a MOOP having two conflicting objectives.

$$\kappa_i = \frac{\frac{f_1^{(i-1)} - f_1^{(i)}}{f_2^{(i-1)} - f_2^{(i)}} + \frac{f_2^{(i+1)} - f_2^{(i)}}{f_1^{(i+1)} - f_1^{(i)}}}{2} \tag{7}$$

where the objectives f_1 and f_2 are considered to be maximized and minimized, respectively.

A solution is said to a stronger knee point if its knee-value is higher than that of the others and vice versa. It is obvious that the knee-zone is most likely to be interesting to the decision maker exclusive of any user's preferences knowledge.

6.1 Non-dominated Sorting Multi-objective Genetic Algorithm (NSGA-II)

Nowadays interest in using of EAs in solving MOOP is increasing by realizing that classical methods possess number drawbacks. Some classical methods are unable to generate the Pareto-front with all possible solutions, particularly in nonconvex-type problems. Sometimes in-depth problem information is needed which is difficult to acquire. Moreover longer computational time for repeated simulation run to identify the Pareto-optimal solution independently is an inherent difficulty of classical methods.

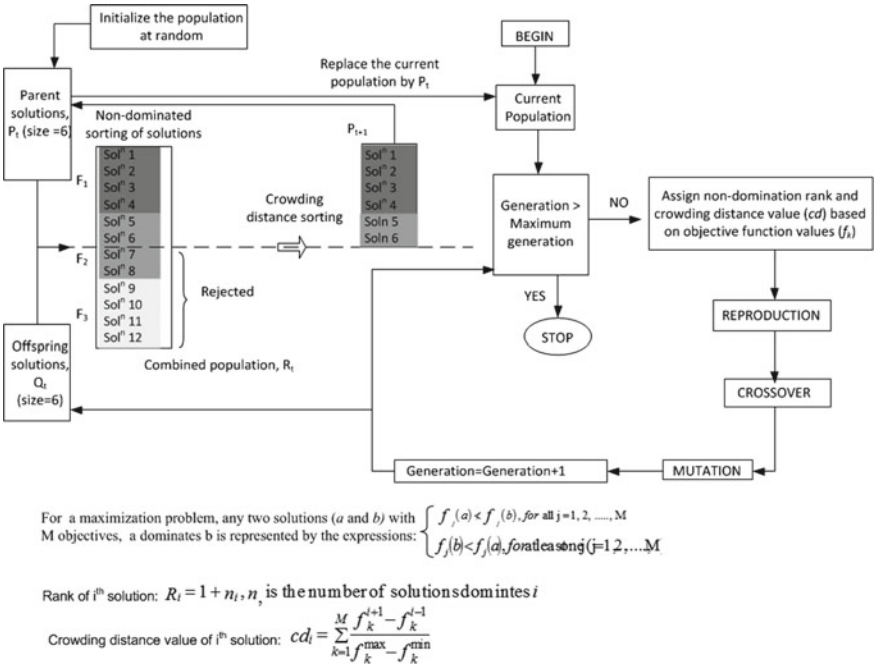

Fig. 4 A schematic presentation of NSGA-II [24]

In contrary, Evolutionary methods are population-based algorithms and have been successfully implemented in many real-world problems having intrinsic complexities in calculating the analytical Pareto-optimal fronts. Earlier efforts of EA implementation in the field of present application [12, 39, 72] confirm its efficacy. In various other real-world problems, EAs are also found to be successfully implemented [22, 28–32, 65, 67, 71, 78]. By realizing that, in the present work, a well-established evolutionary algorithm (EA), NSGA-II (a non-dominated sorting multi-objective genetic algorithm) [24] is considered and its working principle is presented as follows.

Figure 4 demonstrates the working principle of NSGA-II considering binary-coded genetic algorithm (GA). The present demonstration assumes a population size equals six. Present NSGA-II architecture considers crowded tournament selection, polynomial mutation scheme, and simulated binary crossover (SBX). After each GA-generation, six new non-dominated solutions are created. A solution treated as the winner in the tournament should have either lowest rank or larger crowding distance in case of multiple solutions of the same rank.

A generation is started by creating an offspring population Q_t based on the parent population P_t. After that, a collective population, R_t of size 2N is created by combing P_t and Q_t. R_t is then allowed for non-dominated sorting for solution classification based on their ranks. A front is formed by the solutions having the same rank. Figure 4 demonstrates such kind of three fronts (F_1, F_2, and F_3). As the constant population

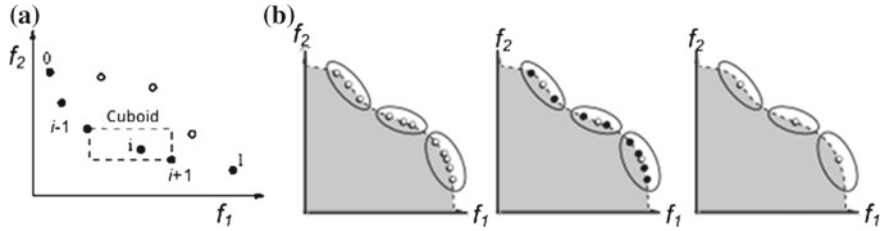

Fig. 5 A schematic representation of **a** crowding distance sorting approach [24], **b** clustering approach [105]

size (= 5) is required to be maintained, forming of the new population (P_{t+1}) is carried out by picking solutions from the different fronts one-by-one starting with the lower rank. The fronts from which no solution is picked are just removed. It may happen that there is a possibility of having more solutions in the final front than the number of solutions just required to reach the population size (= 5) of P_{t+1}. Such a condition happens with F_2 as shown in Fig. 4. In that situation, a niche-preserving strategy (namely crowding distance sorting and clustering approach) is applied to select the required number of solutions from the last front. Considering P_{t+1} as the parent population, P_t, next Q_t was created using the genetic operators, and the same iteration (generation) is allowed to continue until the generation number reaches to a designer specified value.

The crowding distance of an individual is calculated by determining the cuboid length which is equivalent to the summation of the distances of two neighboring solutions from the individual in each objective as demonstrated in Fig. 5a. The mathematical expression to calculate crowding distance (cd_i) is presented in Fig. 4, where M is the number of objectives ($f_{i,\ldots,M}$). Preference of an individual is made with higher crowding distance value.

A schematic representation of the clustering technique is presented in Fig. 5b. In this technique, initially, each solution of the front is treated as the center of the individual cluster. Then two clusters whose distance (which is the Euclidean distance between their centroid) is minimum among that of all cluster pairs are merged to form a single larger cluster, and thereby reducing a cluster from the previous ones. The same procedure of merging two clusters is continued until the number of clusters reaches to the desired number of solutions. For a larger cluster, the solution closest to its centroid is considered and all others are removed.

7 Formulation of Multi-objective Problem for Optimal Trip Planning

Different issues that come to driver's mind while trip planning using EV are mentioned in Sect. 1. In order to know whether EV can reach the destination, an accu-

rate range prediction is necessary. Without considering other reasons (such as EV mechanical structure, road condition, weather, etc.), jerk is responsible for a comfortable journey, and it is required to be minimum during the course of the journey. To reduce the trip time, speed and rates acceleration/deceleration are to be kept high. Reduction of journey cost is achieved by minimizing the overall energy consumption.

Previous studies [9, 18, 55] reveal that deriving harshness have a significant effect on fuel consumptions. In [33], the authors suggest that appropriate changing of driving behavior can reduce the energy consumption considerably. In another study [37], it was suggested that improvement of regenerative braking energy can also be possible by adopting an appropriate deceleration rate. Moreover, the deceleration rate also influences the regenerative braking energy [37]. In some recent works [48, 51, 62, 89], it was revealed that energy requirement during speed changes with constant acceleration rate is found to be more compared to that with multiple acceleration rates. But, the use of multiple acceleration rates increases the jerk that leads to the discomfort [28].

From the above discussions, it is understood that speed, acceleration/deceleration rates, and their durations are the controllable parameters involved to design a trip planning. Whereas, the output parameters (objectives) which are depended on the controllable parameters are cost (energy consumption), range (distance traveled), trip time, and journey comfort. Various works were carried out considering the minimization of trip time as the main objective [60]. A method for prediction of short-term travel duration was proposed based on sensor data from the road in [104]. Moreover, an appropriate driving strategy which highly depends on the road condition is also imperative and it is realized from various studies [9, 18, 33, 55, 88]. Moreover, in order to properly utilize the EV battery's stored energy, it is important that the formulated driving strategy negotiates the predicted range in an optimal manner.

Thus, the driving notion of the driver would be to accelerate the vehicle to reach a speed in the shortest time with adequate comfort while expending the minimum amount of energy possible. In other sense, it indicates that driver would like to accelerate the EV comfortably to a chosen speed with both minimum energy and minimum time. But, these objectives are contradictory to each other, meaning that the improvement of one objective deteriorates the other and vice versa [27, 28].

7.1 Problem Definition

The corresponding MOOP that arises is defined as follows:

$$\text{Minimization of trip time } \left(T_{Trip}\right) = f_T\left(v_{ref}, a_{ref}, k_p, k_i\right) \tag{8}$$

$$\text{Minimization of Energy consumsion } (E) = f_B\left(v_{ref}, a_{ref}, k_p, k_i\right) \tag{9}$$

$$\text{Minimization of average jerk } \left(J_{Avg}\right) = f_{J_{Total}}\left(a_{ref}^{1,2,\ldots,K}, t_{1,2,3,\ldots K-1}, k_p, k_i\right) \tag{10}$$

subject to

$$v_{\min}^{dc} \leq v_{ref} \leq v_{\max}^{dc} \tag{11}$$

$$a_{\min} \leq a_{ref}^{1,2,\ldots,K} \leq a_{\max} \tag{12}$$

$$0.01 \leq k_{pa} \leq 0.3 \tag{13}$$

$$0.01 \leq k_{ia} \leq 3.0 \tag{14}$$

$$0.01 \leq k_{pv} \leq 0.3 \tag{15}$$

$v_{\min}^{dc}$ and $v_{\min}^{dc}$ are the minimum and maximum EV speed (v) limits, respectively. Speed limits depend on the driving cycle (dc) that is currently followed [74] and various safety issues concerning traffic congestion, road condition, weather, location importance such as school, hospital, etc., and so on [2, 56, 66]. $a_{\min}$ and $a_{\max}$ are the minimum and maximum allowable EV accelerations, a related to the EV specification, traffic congestion, road condition, weather, etc. Depending on the EV model type considered, $a_{\min}$ and $a_{\max}$ are taken as 0.1 and 3.0 m/s^2, respectively. k_{pa} and k_{ia} are the proportional and integral gains, respectively, of acceleration controller. k_{pa} was considered to vary in the range 0.01–0.3 and k_{fa} is in the range 0.01, 3.0. The lower and upper values of k_{pv}, velocity controller proportional gain are taken as 0.01 and 0.3, respectively.

In this chapter, the present optimization problem is solved using NSGA-II considering crowding distance approach as a niching strategy discussed in Sect. 6 in finding optimal driving strategies for EV. Since the present application is a constrained optimization problem, the non-dominated solutions are identified based on the superiority approach of the feasible individuals [23].

8 Formulation of Objectives

The proposed DAOTP system is formulated here considering EV model topology introduced in [36, 58, 100]. For the sake of reducing complexity, a simplified model was used. The EV model comprises three major related components: electric motor, battery, and the vehicle dynamics. The acceleration and speed of electric motor were controlled using a proportional–integral (PI) controller and a proportional controller, respectively. The EV model takes the inputs, reference acceleration, a_{ref}, and speed, v_{ref}. The model outputs the objective values after performing several iterations with a certain time step in a simulation process. The simulation was terminated when the reference speed, v_{ref}, was zero indicating the completion of trip, corresponding to n loop iterations. Various model parameters considered for the present study are enlisted Table 1.

Table 1 EV model parameters

Type	DC brushed
Electric motor	
Motor moment of inertia coefficient, I	0.05
Copper losses, kc	0.3
Iron losses, ki	0.01
Windage losses, kw	0.000005
constant electronics losses, $Conl$	600
Proportional controller gain for speed, KP	2.0
Critical motor speed, w_c (rpm)	733
Maximum motor speed, $w_{\max}$ (rpm)	1326
Battery	
Capacity, Cap (A h)	53
Initial state-of-charge, SOC_{init}	1.0
Number of cells in parallel, NP	1
Number of cells in series, NS	76
Type	Lithium-Ion
Voltage, V_P (V)	394
Battery efficiency, $bateff$	0.99
Battery long transient capacitance, $C_{Transient\_L}$ (MF)	0.22375
Battery long transient resistance, $R_{Transient\_L}$ (mΩ)	0.9968
Battery short transient capacitance, $C_{Transient\_S}$ (MF)	0.03518
Battery short transient resistance, $R_{Transient\_S}$ (mΩ)	0.9338
Battery series resistance, R_{Series} (mΩ)	1.4932
Vehicle	
Air density, ρ_{air} (kgm^3)	1.143
Frontal Drag coefficient, C_D	0.19
Back Drag coefficient, C_{D_back}	0.3
Frontal area, A_f (m^2)	1.8
Back area, A_b (m^2)	1.4
Gravitational acceleration, g (ms^2)	9.81
Mass including passengers and drivers, m (kg)	1460
Overall gear ratio/tire radius, G (m^{-1})	37
Rolling resistance coefficient, μ	0.014
Transmission	Single-speed
transmission efficiency, $geff$	0.95
Regenerative braking factor, $Rgen$	0.5

8.1 Electric Motor Model

The motor model's inputs Various parameters such as battery voltage, V_P, reference acceleration, a_{ref}, vehicle real acceleration, a, reference speed, v_{ref}, vehicle real speed, v, and rotational speed, w, are considered as the inputs to the motor model. The outputs are the battery current, I_P, and electric motor torque, τ.

The speed error defined in Eq. (2) is rewritten for the ith loop iteration as

$$e(i) = v_{ref} - v(i) \tag{16}$$

The acceleration error defined in Eq. (4) is rewritten for the ith loop as

$$f(i) = a_{ref} - a(i) \tag{17}$$

The switching function, SF of the motor is determined as follows:

$$\begin{aligned} SF(i) &= k_p f(i) + k_i\, f_{\text{int}}(i), \ \text{if e(i)} < f_{sa} \cdot v_{ref} \\ SF(i) &= KP \cdot e(i) \text{ and } f_{\text{int}}(i) = 0, \quad \text{otherwise} \end{aligned} \tag{18}$$

where f_{sa}, switching factor from speed to acceleration controller was taken to be 0.02. $f_{\text{int}}(i)$ is the integral of acceleration error which is defined by $f_{\text{int}}(i-1) + f(i) * dt$ and $f_{\text{int}}(0) = 0$.

The switching function value found using Eq. (18) is saturated as follows to calculate the motor torque.

$$SF(i) = \left.\begin{matrix} 1 \\ -1 \\ SF(i) \end{matrix}\right\} \begin{matrix} \text{if } SF(i) > 1 \\ \text{if } SF(i) < -1 \\ \text{otherwise} \end{matrix} \tag{19}$$

The torque needed from the motor is

$$\tau(i) = SF(i) \cdot \tau_{\max}(i) \tag{20}$$

where τ_{max} is the maximum torque that can be safely developed by the motor and its value is decided according to Eq. (21).

$$\left.\begin{matrix} \tau_{\max}(i) = 140 \\ \tau_{\max}(i) = 9.1274 \\ \tau_{\max}(i) = \frac{102000}{w(i-1)} \end{matrix}\right\} \text{if} \begin{matrix} w(i-1) \le w_c \\ w(i-1) \ge w_{\max} \\ w_c < w(i-1) < w_{\max} \end{matrix} \tag{21}$$

The units are N-m. The motor current, $I_M(i)$ is

$$I_M(i) = \frac{\tau(i) \cdot w(i)}{V_P(i-1)} \tag{22}$$

Now, the motor efficiency, *effmotor*, is calculated by Eq. (23).

$$effmotor\,(i) = \frac{\tau(i) \cdot w(i)}{\tau(i) \cdot w(i) + \tau(i)^2 \cdot kc + w(i) \cdot ki + w(i)^3 \cdot kw + Conl} \tag{23}$$

The above-calculated motor efficiency was saturated as follows:

$$effmotor(\mathrm{i}) = \left.\begin{array}{c} 1 \\ -1 \\ effmotor(\mathrm{i}) \end{array}\right\} \begin{array}{c} \text{if } effmotor(\mathrm{i}) > 1 \\ \text{if } effmotor(\mathrm{i}) < -1 \\ \text{otherwise} \end{array} \tag{24}$$

The effective motor current $I_{M\_eff}(i)$ is derived from the motor current, $I_M(i)$ and considering the *effmotor* and *conveff* (converter efficiency), as follows:

$$\left.\begin{array}{l} I_{M\_eff}(i) = \frac{I_M(i)}{conveff \cdot effmotor(i-1)} \\ I_{M\_eff}(i) = I_M(i) \cdot conveff \cdot effmotor(i-1) \cdot Rgen \end{array}\right\} \text{if } \begin{array}{c} SF(i) > 0 \text{ and } v_{ref} \neq 0 \\ SF(i) < 0 \end{array} \tag{25}$$

The regenerative braking factor, *Rgen*, is the fraction of the total available regenerative energy that is converted to battery energy.

8.2 Battery Model

The lithium-ion battery model presented in [19] is adopted here. Battery current, I_P, is the input of battery model. The model's outputs are V_P, and battery state-of-charge, *SOC*.

Considering the maximum and minimum limits of battery current, the battery current to be calculated using the revised motor current is as follows:

$$I_P(i) = \left.\begin{array}{c} I_{M\_\max} \\ I_{M\_\min} \\ I_{M\_eff}(\mathrm{i}) \end{array}\right\} \begin{array}{c} \text{if } I_{M\_eff}(i) > I_{M\_\max} \\ \text{if } I_{M\_eff}(i) < I_{M\_\min} \\ \text{otherwise} \end{array} \tag{26}$$

Here, $I_{M\_\max}$ and $I_{M\_\min}$ are considered as 400 and −400 A. Considering the battery efficiency and mode of EV speed change (acceleration/deceleration), the effective battery current, $I_{P\_eff}(i)$ can be derived from battery current, $I_P(i)$ defined in Eq. (26) as follows:

$$\left.\begin{array}{l} I_{P\_eff}(i) = \frac{I_P(i)}{bateff} \\ I_{P\_eff}(i) = I_P(i) \cdot bateff \end{array}\right\} \text{if } \begin{array}{c} SF(i) > 0 \\ SF(i) \leq 0 \end{array} \tag{27}$$

The current flowing through an individual cell is

$$I_{cell}(i) = \frac{I_{P\_eff}(i)}{N_P} \tag{28}$$

The battery SOC is calculated as

$$SOC(i) = SOC(i-1) - \int \frac{I_{cell}(i)}{Cap}\, dt \tag{29}$$

The initial value of $SOC(i)$ is the so-called initial state of charge of the battery, SOC_{init}. The battery voltage is

$$V_P(i) = N_S V_{cell}(i) \tag{30}$$

where V_{cell} is the voltage of an individual cell. Based on the Kirchhoff's Current Law, the voltage of $C_{Transient\_L}$ is calculated as

$$\frac{d}{dt}\big(V_{C\_L}(i)\big) = \frac{I_{cell}(i)}{C_{Transient\_L}} - \frac{V_{C\_L}(i)}{C_{Transient\_L} R_{Transient\_L}} \tag{31}$$

and the voltage of $C_{Transient\_S}$ is

$$\frac{d}{dt}\big(V_{C\_S}(i)\big) = \frac{I_{cell}(i)}{C_{Transient\_S}} - \frac{V_{C\_S}(i)}{C_{Transient\_S} R_{Transient\_S}} \tag{32}$$

The open-circuit voltage is calculated as

$$V_{OC}(i) = -1.031e^{(-35SOC(i))} + 3.685 + 0.2156SOC(i) - 0.1178SOC(i)^2 + 0.3201SOC(i)^3 \tag{33}$$

The voltage of an individual cell is determined as

$$V_{cell}(i) = V_{OC}(i) - V_{C\_S}(i) - V_{C\_L}(i) - I_{cell}(i)R_{Series} \tag{34}$$

8.3 Vehicle Dynamics Model

The electric motor torque, τ, the model input, and the model's outputs are a, v, and R, and the rotational speed, w. The aerodynamic drag force acting on the EV is

$$F_D(i) = \frac{1}{2}\rho_{air} A_f C_D v(i)^2 \tag{35}$$

The frictional force between the road and wheel is

$$F_{rr}(i) = \mu mg \tag{36}$$

The traction force supplied by the motor is

$$F_t(i) = \tau(i)G \cdot geff \tag{37}$$

Force caused by road gradient is

$$F_{gra}(i) = \sin\left(\frac{grad \cdot \Pi}{180}\right) \cdot mg \tag{38}$$

Force caused by the vehicle inertia is

$$F_{inertia}(i) = I \cdot m \cdot a(i) \tag{39}$$

Considering the wind velocity and its direction (with respect to vehicle movement) effect into the drag force [40], and assuming all the braking force come from the electric motor, the acceleration is

$$a(i) = \frac{\tau(i) \cdot G \cdot geff + \frac{1}{2}\rho_{air} A_b C_{D\_back} \left(v(i) - v_{wind \cdot \cos(\theta_{wind})}\right)^2 - \mu mg - \sin\left(\frac{grad \cdot \Pi}{180}\right) \cdot mg - I \cdot m \cdot a(i)}{m},$$
$$\text{if } v_{wind} > v(i) \text{ and } 270° < \theta_{\text{wind}} < 90° \tag{40}$$

$$a(i) = \frac{\tau(i) \cdot G \cdot geff - \frac{1}{2}\rho_{air} A_f C_D \left(v(i) - v_{wind \cdot \cos(\theta_{wind})}\right)^2 - \mu mg - \sin\left(\frac{grad \cdot \Pi}{180}\right) \cdot mg - I \cdot m \cdot a(i)}{m},$$
$$Otherwise \tag{41}$$

where θ_{wind} (in degree) ($0° < \theta_{\text{wind}} < 360°$) is the wind velocity angle measured with respect to the EV movement direction, grad (in degree) is the road gradient (it becomes negative if the road is downhill, and positive if the road is uphill), ρ_{air} is the air density at the EV's current location.

The EV speed can be calculated using.

$$v(i) = v_{i-1} + \int a(i)\, dt \tag{42}$$

ω is given by

$$\omega(i) = v(i)G \tag{43}$$

The distance traveled by EV, $x(i)$ is given by

$$R(i) = R(i-1) + v(i)\, dt \tag{44}$$

The objective functions are defined as follows:

$$T_{Trip} = n \cdot dt \tag{45}$$

$$E = \sum_{i=1}^{n} I_P(i) V_P(i) \tag{46}$$

$$j_i = \frac{a(i+1) - a(i)}{dt} \tag{47}$$

$$J_{Avg} = \frac{\sum_{i=1}^{n_d} j_i}{n_d} \tag{48}$$

where j_i is the jerk experienced for a time step, dt due to change of acceleration. J_{Avg} is the average jerk value calculated based on jerks (j_i) that are found to be greater than the desired value, J_{desire} (i.e., $j_i > j_{desire}$). This automatically excludes very low values of jerk due to controller or simulation conditions.

8.4 EV Simulation

The EV simulation is carried out starting from its present speed (v_{init}) with multiple accelerations for a time period (D_{acc}) to reach to the desired reference speed (v_{ref}). Once the speed reaches close to v_{ref} (say 99%), switching from acceleration controller to speed controller is made, and vice versa depending on the driving mode. The EV jerk was recorded at the end of each time interval. The EV energy consumption (E_{acc}), total jerk (J_{Total}), trip time, T_{Trip} and range (R_{a}) were calculated at the simulation end. By plotting the values of different objectives, a non-dominated front (i.e., Pareto front) was obtained. The termination criteria of the EV simulation was to satisfy any one of the following:

$$\left.\begin{aligned} &SOC \leq 0.2 \\ &x \geq Range_{Trip} - 10 \\ &v_{\text{End of trip}} \leq 5 \text{ kph} \end{aligned}\right\} \tag{49}$$

According to the Road Safety Authority (RSA), to stop or slow down a vehicle, braking should be applied while accounting for a minimum stopping distance from the stopping point or from the location of the start of a speed limit lower than the present one. The total stopping distance (TSD) is normally the summation of the driver's reaction distance and the braking distance, and it also depends on the dryness or wetness of the road surface [31]. TSD increases exponentially with the current vehicle speed. For the sake of simplicity, a linear relationship is considered here. In the present context, when the residual trip distance is less than a minimum TSD (Trip End Safety Distance for braking (*TESDB*) approached to stop the vehicle), the current EV speed reference becomes $v_{\text{End of trip}}$. *TESDB* is calculated using Eq. (50).

$$TESDB = dec\_factor\_safety \frac{v^2_{\text{ref\_trip end}}}{2 \cdot a_{\text{dec}}} \tag{50}$$

where a_{dec} (m/s^2) is calculated using Eq. (51) based on v_{diff_dec} (m/s), the difference between the desired speed after deceleration and the current EV speed. *dec_factor_safety* is the safety parameter used during deceleration mode to ensure that the vehicle slows down or stops within the allowable distance. The deceleration (a_{dec}) was assumed depending on $v_{\text{diff\_dec}}$ as follows:

$$\begin{matrix} a_{dec} = 2.3 \\ a_{dec} = 2.25 \\ a_{dec} = 2.35 \end{matrix} \quad \text{if} \quad \begin{cases} 100 \leq v_{diff\_dec} \leq 129 \\ 50 \leq v_{diff\_dec} \leq 100 \\ 0 \leq v_{diff\_dec} \leq 50 \end{cases} \tag{51}$$

According to the micro-trip presented in Fig. 2, $v_{\text{ref\_trip end}}$ in Eq. (50) refers to v_{ref3}.

9 Results and Discussions

9.1 Neighborhood Micro-trip Planning

The results of the DAOTP system in the present work are presented based on a few assumptions as follows. The speed limits are chosen only based on the corresponding driving cycle followed by EV. The safety factors such as safe following distance, etc., related to traffic congestion, road condition, weather, location importance, etc., are not considered while fixing the EV speed limits for the sake of simplicity. Other assumptions concerning accelerations limits, model parameters, etc., have been mentioned in the previous sections. In this study, other trip parameter values considered are depicted in Table 2.

Moreover, the applied micro-trip is simple in the sense that it follows only one driving cycle type for the entire trip length. The velocity profile versus distance of a simple micro-trip consisting of one driving cycle type is presented in Fig. 6. The simple micro-trip consists of one acceleration mode followed by a constant speed model within the speed limits of the driving cycle, and after that, the EV comes to a

Table 2 Values of different parameters considered during simulation process

Parameters	Value
dt (in, s)	0.01
Auxiliary load (in, J/s)	10500
SOC_{init}	1.0
J_{desire}	1.0
K	2
dec_factor_safety	1.25

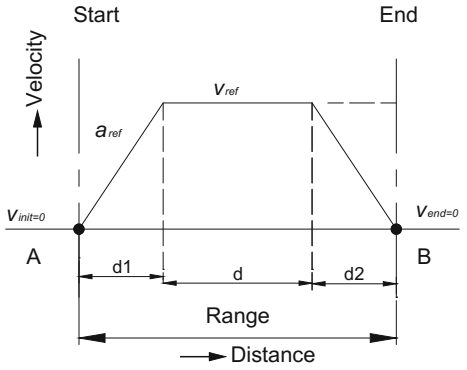

Fig. 6 Velocity versus distance plot of a simple micro-trip consisting of one driving cycle

Table 3 Values of GA parameters

GA Parameters	Value
N	250
Mutation probability	1/length of chromosome
Crossover probability	0.985
No. of bits used for each variable	20
Random seed	0.4
Number of generation	100

stop during the deceleration mode. The values of GA parameters presented in Table 3 are used for MOO process throughout this chapter unless otherwise stated.

In an urban area, depending on the vehicle speed limits, two driving cycle types, neighborhood (v_{erf} is varying from 8 to 40 km/h), and urban (v_{ref} is varying from 40 to 56 km/h) are applicable.

Figure 7 presents the Pareto fronts achieved by DAOTP after solving the MOOP (defined in Sect. 7) for minimization of energy consumption, trip time, and average jerk in the neighborhood driving cycle are presented in Fig. 7. In this figure, the Pareto fronts are shown for six different trip lengths (ranging from 0.5 to 20 km) keeping the other parameters related to the route (presented in Table 4) fixed. The wind angle is measured based on the same coordinate system as followed by the vehicle. That is, if the direction of the wind and the vehicle are the same, the wind angle equals zero.

In Fig. 7, Pareto front spans in all three objectives (energy, trip time, and average jerk) were observed to be dissimilar for dissimilar trip length, as anticipated. With increasing the trip length, the Pareto fronts are found to be migrated gradually move away from the origin. Among the six chosen trip lengths, some optimal solutions of trip lengths especially, 5, 8, and 10 km are found to be of a very low average jerk (less than 4 m/s^3), longer trip time and more energy consumption. On the other hand, few solutions of trip length (in particular, 0.5 and 5 km) possess a very high average

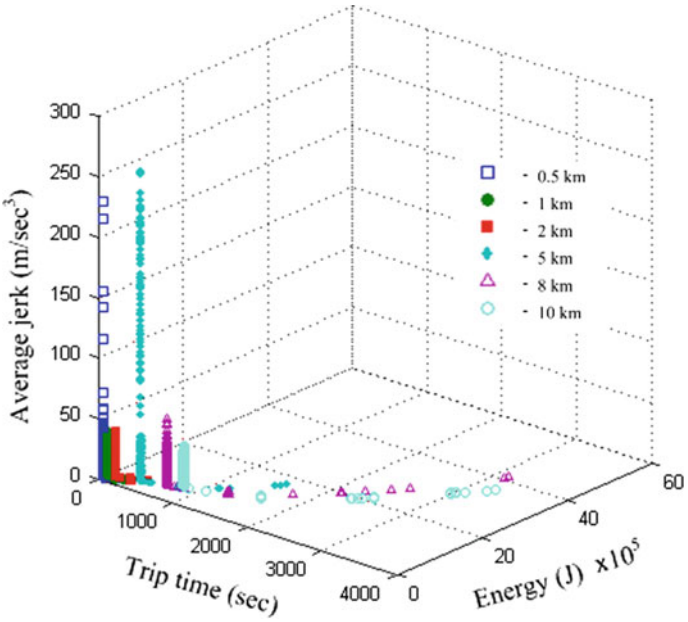

Fig. 7 Pareto-optimal fronts obtained in solving MOOP defined in Sect. 7 in neighborhood driving

Table 4 Route characteristic data

Sr. No.	Distance		Route characteristic parameters	
			Road gradient	
	From	To	Value	Angle (°)
1	0	Trip end	0	–
			Rolling frictional coefficient of road surface	
2	0	Trip end	0.015	–
			Density of air	
3	0	Trip end	1.143	–
			Wind velocity (km/h)	
4	0	Trip end	0	0

jerk value (more than 100 m/s^3) with short trip time and low energy consumption. It is obvious that such kind of solutions having extreme objective values is not to be attractive to the driver. By realizing this, Pareto-optimal solutions are screened by limiting the average jerk values in the range, 4–100 m/s^3, and the revised fronts are shown in Fig. 8. It is interesting to observe that as the trip length increases, less number of solutions outside the above mentioned average jerk limit belong to the Pareto front. This is to be expected since the definition of average jerk involves

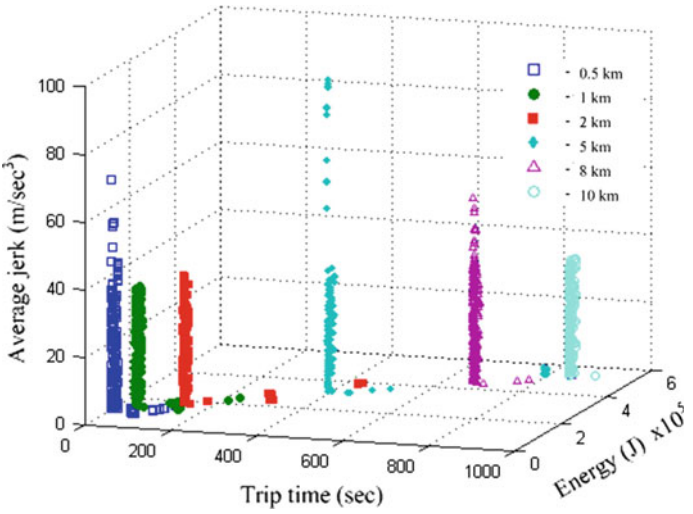

Fig. 8 Revised Pareto-optimal fronts based on average jerk limits (4 m/s^3 < average jerk < 100 m/s^3) in neighborhood driving cycle for different simple micro-trip length

dividing by the number of times (n_d) the jerk exceeds a certain limit (J_{desire}) according to Eq. (48). Since there is only one acceleration mode for all the micro-trips in Fig. 8, the average jerk is expected to generally decrease as the trip length increases. n_d increases, but j_i is found to be low when the EV runs at a constant speed.

The amount of energy stored in a battery is realized by knowing its SOC, and it can easily measure and presented to the driver through a suitable device based on based on multi-modal electrochemical impedance spectroscopy [73] and also easily interpreted by the driver. Thus, instead of actual energy utilization, it is more expedient for a driver to know the associated residual battery SOC. For that reason, the optimization results are discussed here in terms of SOC value at the end of the trip (*SOC*) and the trip time.

In Fig. 9, plot of *SOC* versus trip time for the 0.5 km micro-trip is presented. It is observed that after a certain trip time, *SOC* is found to be decreasing with increasing trip time because of a low jerk. It is evident that though the average jerk is low, such kind of solutions is not attractive at all. Instead solutions with a high *SOC* or a low trip time will be more interesting. A dotted ellipse in Fig. 9 shows the most attractive portion of the *SOC*-trip time plot and the corresponding solutions are replotted in Fig. 10. Though these solutions are non-dominated with respect to the original (three) objectives, are not non-dominated with respect to *SOC* and trip time. As a result, a one-to-one *SOC*-trip time plot is not anticipated. Figure 10 shows that *SOC* decreases with increasing time because the energy consumption is inversely varying with time. The variation of energy consumption with *SOC* is also demonstrated in Fig. 10. The energy consumption is found to be linearly varying with

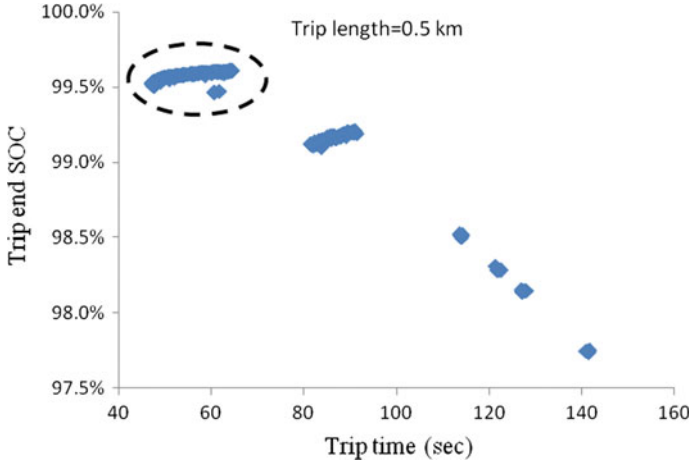

Fig. 9 Variation of end SOC with trip time in 0.5 km range

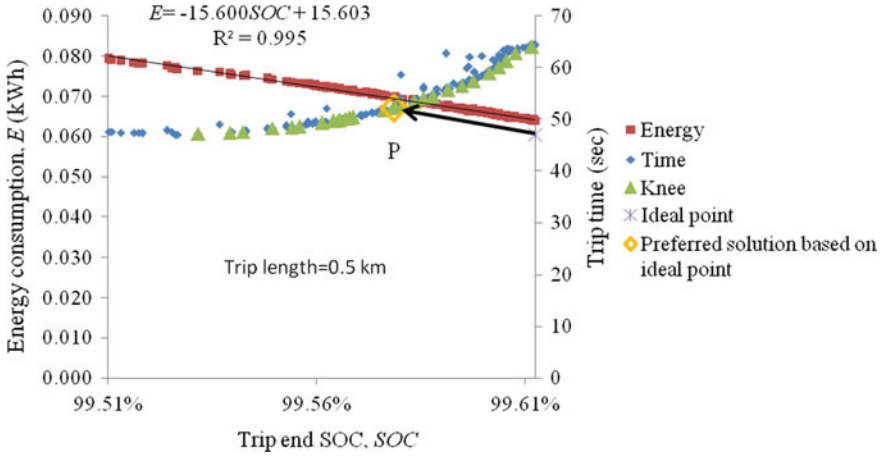

Fig. 10 Range-SOC-time plot corresponding to a micro-tip of 0.5 km

SOC with a gradient of −15.6. The empirical linear equation with a corresponding the coefficient of determination (R^2) value is depicted in the Fig. 10.

Similar studies on the variation of *SOC* with trip time were conducted for the other trip lengths. Figure 11 is similar to Fig. 9 except that the solutions correspond to the 5 km micro-trip. Considering the interesting part of the plot based on the relationship between SOC and time, the trip end SOC (*SOC*) versus trip time plot is presented in Fig. 12. It also shows the energy consumption of the interesting solutions. The linear relationship of energy with *SOC* is depicted in the Fig. 12 and has a high R^2 value, just like Fig. 10. Moreover, after analyzing the energy and trip end SOC relationships of trip lengths 0.5 and 5 km as shown in Figs. 10 and 12, as well as that found in

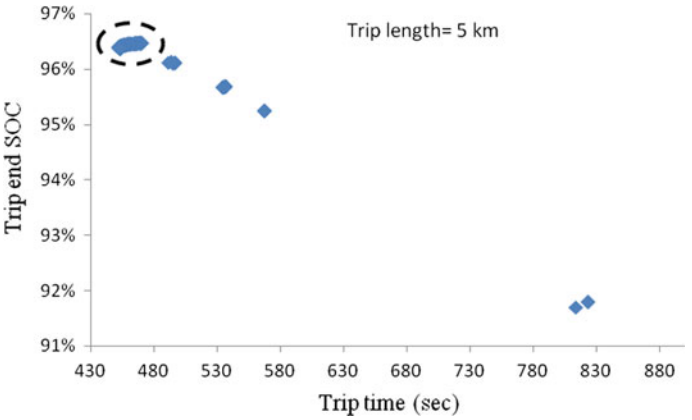

Fig. 11 Variation of trip end SOC with trip time for 5 km trip

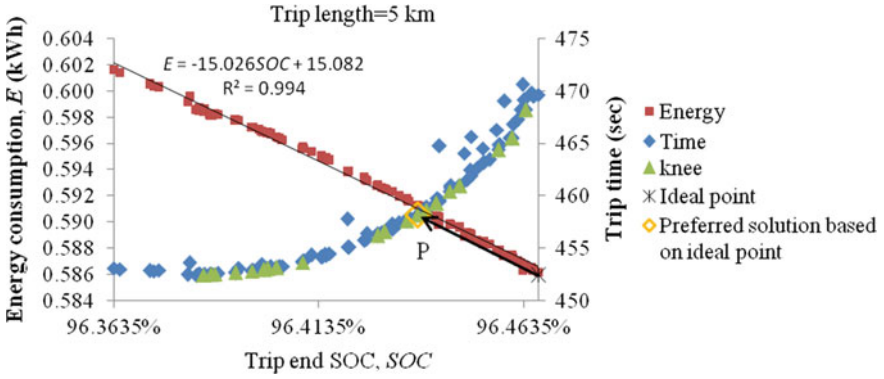

Fig. 12 Energy–*SOC*–time plot corresponding to a micro-tip of 5 km

other trip lengths, it was found that the slopes and intercepts are very close up to a trip length of 10 km with standard deviations, 0.22 and 0.20, respectively. After taking a mean value of both slope and intercept, a generalized linear relationship among (kWh) and *SOC* (0–100%) the optimal solutions defined in Eq. (52) may be applicable up to 10 km trip length for the present EV model.

$$E = -15.4245SOC + 15.464 \tag{52}$$

After 10 km trip length, the slope and intercept were found to be different and less than that in Eq. (52).

Figure 10 and Fig. 12 present the initial twenty knee-points evaluated using Eq. (7) for the trip lengths 0.5 km and 5 km, respectively. The reference point based preferred solutions for these trip lengths are also depicted in Fig. 10 and Fig. 12, respectively. The ideal (reference) point based preferred solution is found to be one of the twenty

knee points, and it is observed in both the trip lengths. However, it is not always true. An example is the case of 8 km trip length (not shown in the chapter).

Values of the three objectives, decision variables, and *SOC* are shown in Table 5. As mentioned in Sect. 8, a deceleration safety factor (presented in Table 2) was considered during braking the EV to ensure that the vehicle stopped before or close to the trip end location. Now, depending on the EV speed the *TESDB* is varied. Thus, instead of the same trip length (assumed prior to the trip), each solution possesses a different distance but always close to the desired trip length. The actual range covered corresponding to the optimal solution is also enlisted in Table 5. Prior to the initiation of the journey, DAOTP evaluates the optimal driving strategies in different driving modes for the entire trip in an offline mode based on the route information and battery SOC. According to the DAOTP predictions, the driver makes a decision for his/her trip planning. After starting the trip, DAOTP begins evaluating the new (revised) optimal driving strategy in every (certain) time interval according to the current EV state and route characteristic data in online mode till the trip ends. This online suggestion of DAOTP accounts for any deviation from the initial optimal driving strategy due to unforeseen circumstances or a lack of concentration by the driver. In such circumstances, the driver will be notified right after a time interval by comparing the previous and present DAOTP predictions. The subsequent driving strategies will be very similar to the previous strategy if the deviation applied driving strategy from the predicted is minor.

In both the trip lengths (0.5 and 5 km), it was found that the optimal speed is close to the maximum speed limit of neighborhood driving cycle (40 km/h). The variation of EV speed with trip end SOC of the Pareto-optimal solutions found in 0.5 km trip is presented in Fig. 13. About 94% of the solutions possess the speed around 40 km/h, which is the speed limit. From Table 5, it was noticed that in both trip lengths, the first acceleration value is found to be higher than the second acceleration value. On the other hand, the first acceleration's duration was found to be lower than that of the second acceleration. The variations of EV accelerations and acceleration durations with trip end SOC found in the 0.5 km trip length are presented Fig. 14. In Fig. 14, the first accelerations of nearly all Pareto-optimal solutions are observed to be similar, and possessed a high value (close to the upper limit of the acceleration range presented in Eq. (12)). On the other hand, the second acceleration is increasing with increasing the trip end SOC with a second-order polynomial relationship (with a coefficient of determination, $R^2 = 0.9773$) defined by Eq. (53). Similarly, the duration of first acceleration of the Pareto-optimal solutions was found to be a constant value close to 1.65 s and that of the second acceleration to be varying with trip end SOC according to Eq. (54) with a coefficient of determination, $R^2 = 0.95$.

$$a_2 = 5.279 \times 10^6 \mathrm{SOC}^2 - 1.051 \times 10^7 \mathrm{SOC} + 5.236 \times 10^6 \tag{53}$$

$$t_2 = 1.01 \times 10^8 \mathrm{SOC}^2 - 2.01 \times 10^8 \mathrm{SOC} + 9.99 \times 10^7 \tag{54}$$

After conducting the similar innovation study for trip length 5 km, it was observed that the first acceleration value and corresponding duration of the Pareto-optimal

Table 5 Preferred optimal solutions obtained using reference point based method in neighborhood micro-trip

Trip length (km)	Ideal point according to SOC–Time plot	Optimal values of objectives	Optimal values of decision variables					Actual range covered, R	Preferred Pareto-optimal solution
			V	a_k	t_k	k_p	k_i		
0.5	SOC = 0.996084; Time = 47.038	T_{Trip} = 52.1573; E = 251006; J_{Avg} = 22.614	39.994	a_1 = 2.99542; a_2 = 0.321796	t_1 = 1.65767; t_2 = 19.1627	0.222576	0.707864	485.981	Denoted as "P" in Fig. 10
5	SOC = 0.964669; Time = 452.430	T_{Trip} = 458.166; E = 2128720; J_{Avg} = 34.8546	39.9992	a_1 = 2.94564; a_2 = 0.289447	t_1 = 1.68578; t_2 = 21.2146	0.245648	0.730512	4985.99	Denoted as "P" in Fig. 12

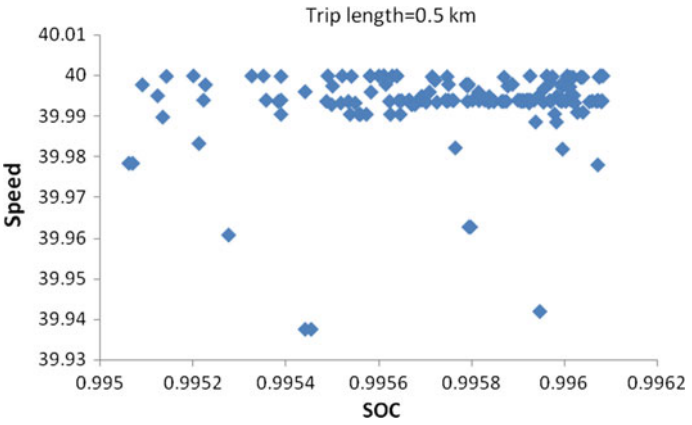

Fig. 13 Variation of EV speed with SOC in 0.5 km range

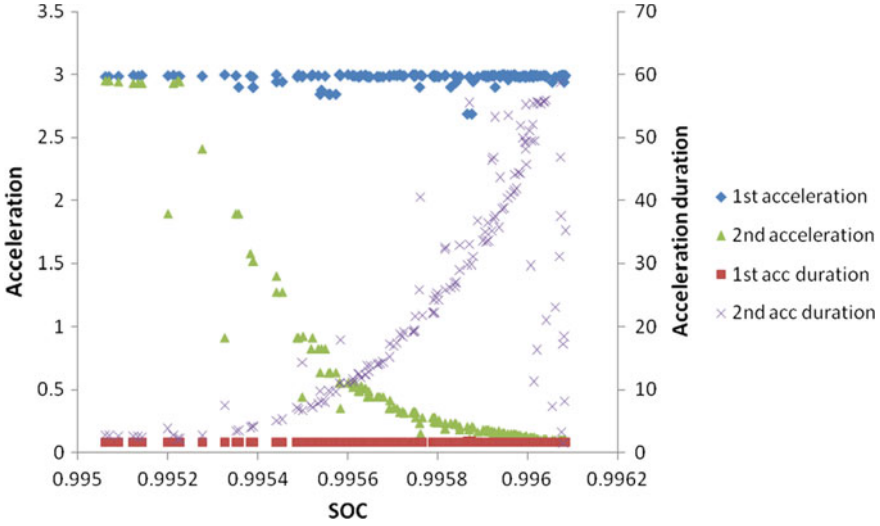

Fig. 14 Variations of EV accelerations and acceleration durations with SOC in 0.5 km range

solutions are found to be the same as observed in the case of trip length, 0.5 km. The relationships of the second acceleration and its duration with trip end SOC are also found to be a second-order polynomial defined by Eqs. (55) and (56) corresponding to the coefficients of determination (R^2), 0.9865 and 0.9826, respectively. The difference between the coefficient values of the corresponding relationships of trip length 0.5 and 5 km are found to be negligible. This suggests that the acceleration strategies are found to be almost similar nature irrespective of the trip length in neighborhood micro-trips. This implies that the migration of the Pareto fronts in Fig. 9 that was

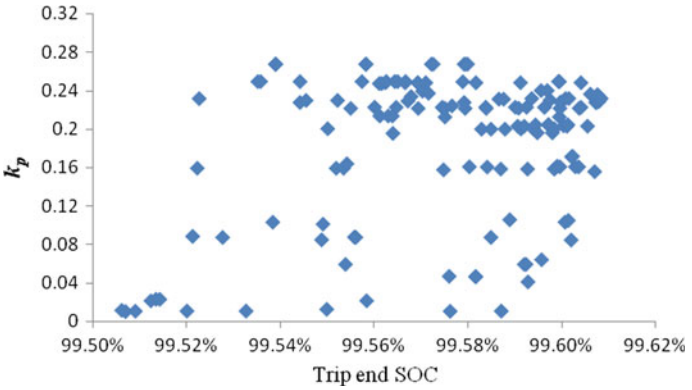

Fig. 15 Variation of k_p with trip end SOC in 0.5 km range

alluded to previously in this section is solely due to the duration of constant speed mode dictated by the trip length.

$$a_2 = 6.458 \times 10^6 \mathrm{SOC}^2 - 1.246 \times 10^7 \mathrm{SOC} + 6.007 \times 10^6 \tag{55}$$

$$t_2 = 1.046 \times 10^8 \mathrm{SOC}^2 - 2.016 \times 10^8 \mathrm{SOC} + 9.715 \times 10^7 \tag{56}$$

After analyzing the variations of k_p and k_i with trip end SOC, as presented in Figs. 15 and 16, respectively, it was noticed that most of solutions are lie within a particular region. In the case of trip length 0.5 km, k_p is varying from 0.2 to 0.25 and k_i, from 0.3 to 0.8; 67% and 62%, respectively, of the entire solutions are within these ranges. Similarly, k_p and k_i values of most of the Pareto-optimal solutions obtained in higher trip lengths vary with certain ranges. However, from Table 5, a comparatively high value of both k_p and k_i was found in the preferred solution with higher trip length.

Table 6 shows the energy savings that are achieved on various trips. The % energy savings are evaluated based on the minimum and maximum energy consumptions of the interesting solutions as found after optimization process. Such energy savings can be obtained by sacrificing the corresponding trip duration. The maximum and minimum energy consumption, the lowest value of trip end *SOC*, and its effective range found among the optimal solutions corresponding to a trip length are also enlisted in Table 6. Like energy saving, the % trip time in the fourth column of Table 6 are also calculated corresponding to the minimum and maximum time required to complete the trips. From Table 6, it was observed that the energy saving reduces with increasing the trip length. However, the energy saving per unit trip time lost is getting more as the trip length increases (e.g., 0.46 and 1.06, in trip length 0.5 and 10 km, respectively). The following describes a scenario that highlights the versatility of the proposed DAOTP system and possible energy savings among the obtained Pareto front solutions in exchange for sacrificing trip time. For the sake of demonstration,

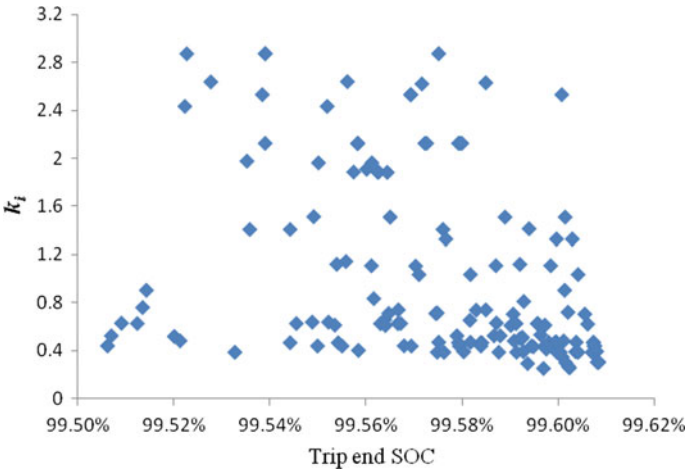

Fig. 16 Variation of k_i with trip end SOC in 0.5 km trip length

Table 6 Energy saving corresponding to time lost for different neighborhood micro-trip length

Trip length (km)	Maximum energy consumption (kwh)	Minimum energy consumption (kwh)	Energy saving (%)	Trip time lost (%)	Lowest SOC (%)	Effective SOC range (%)
0.5	0.07326	0.06507	12.581	27.14	99.5062	0.1022
1	0.13717	0.12221	12.237	21.14	99.1587	0.0986
2	0.25265	0.23817	6.078	9.76	98.464	0.096
5	0.60166	0.58616	2.644	40.22	96.3635	0.1034
8	0.96582	0.93420	3.385	2.67	94.169	0.1985
10	1.23428	1.16499	5.947	5.59	92.5536	0.4233

the solutions having maximum energy consumption are supposed to be suboptimal, considered to be obtained without DAOTP. On the other hand, the solutions having minimum energy consumption are considered to be the best DAOTP solutions. This demonstration should not be confused with selection criteria (decision-making techniques/driver preference) of a DAOTP solution for implementation.

In a downtown area where the neighborhood driving cycle is normally followed, the vehicle is required to stop frequently due to more traffic congestion and traffic lights. As a result, to cover a trip length, the vehicle breaks the entire trip length into multiple micro-trips, the beginning and end of which correspond to two successive stops. After analyzing the data presented in Table 6, it was found that there will be 6.82% $(=(0.07326 \times 2 - 0.13717) \times 100/0.13717)$ more energy consumption if the EV runs 1 km with a stop after every 0.5 km compared to traveling the same distance at a stretch without adopting the optimized driving strategy. This energy consumption can be reduced to 5.12% $((0.06507 \times 2 - 0.13717) \times 100/0.13717)$ if

DAOTP results are followed during the journey with breaks. So, there will be a saving of up to 1.70%. (=6.82–5.12). For more number of stops in a trip length, the saving is more. For instance, the extra energy loss to travel 5 km distance with a stop after every 0.5 km traveled instead of a continuous journey and without adopting DAOTP results is 21.76%. This excess energy consumption comes down to 8.15% if DAOTP results are adopted and the saving of energy will be up to 13.61%. corresponding to 2.722% per km. If in both cases (continuous and journey with stops) DAOTP results are utilized, the amount of energy loss will be reduced from 21.76% to 11%, and 6.82% to 6.48%, for trip lengths 5 km and 1 km, respectively, with a stop after every 0.5 km. The above study reveals that the benefits of adopting DAOTP system during performing a trip with EV.

9.2 Urban Micro-trip Planning

Similar studies were conducted on DAOTP application in urban micro-trips (speed range 40–56 km/h) for the same six trip lengths as considered in neighborhood driving cycle. The nature of Pareto fronts found was found similar to that of the neighborhood driving cycle. The interesting solutions in a Pareto front were identified following the concept based on the problem-specific information that was adopted in the neighborhood driving cycle. The relationship between E and SOC was found to also be linear. The generalized linear relationship derived after averaging the slope and intercept found in six trip lengths is presented in Eq. (57). The standard deviations of the slope and intercept in different trip lengths were found at 0.25 and 0.24, respectively. These are slightly lower than the slope and intercept values for neighborhood trips.

$$E = -14.871SOC + 14.995 \tag{57}$$

The preferred solution was found out using the reference point technique based on the ideal point. In Table 7, values of optimum decision variable of the preferred solutions found in urban micro-trips of lengths 0.5 and 5 km, along with the corresponding objectives, actual range covered and the respective ideal point used are listed. After comparing the data of Tables 5 and 7, a similarity in the optimization results was for the optimal speed, both the acceleration values and the first acceleration duration for both the trip lengths. However, in urban driving cycles, it was found that for the 0.5 km trip length, the optimal value of the second acceleration duration is low compared to that in the neighborhood driving cycle. This happens because since the trip length is short so that before reaching the optimal speed, the EV covers the trip length. Due to this reason, a smooth plot of the second acceleration duration with trip end SOC (as seen in the neighborhood driving cycle, Fig. 14 corresponding to trip length, 0.5 km) may not be expected through a similar nature of the relationship of the second acceleration value with trip end SOC was observed. As the trip length increases, similar results as observed in the neighborhood driving

cycle can be anticipated in the urban driving cycle as well. Moreover, a significant difference in the k_p and k_i was found. In the higher speed driving cycle, the optimum values of those variables reduce with increasing trip length.

The above DAOTP results are found based on the route characteristic data presented in Table 4 and considering an initial battery SOC of 100%. Changes of route characteristic parameters and a different initial battery SOC may affect the DAOTP results. The effectiveness of route characteristic parameters, such as road gradient, road surface condition, wind velocity, elevation, and battery initial SOC on DAOTP results are investigated in highway micro-trips planning.

9.3 Highway and Interstate Micro-trip Planning

Results for high-speed driving cycles are presented here for seven trip lengths ranging from 1 to 50 km. The trips are considered based on the structure of a simple micro-trip as shown in Fig. 6. The same EV model and related model parameter values as mentioned above are adopted here. By solving the associated MOOP (presented in Sect. 7 of the first part), a smooth Pareto front surface was found for each trip length in both high-speed driving cycles, highway and interstate, as shown in Figs. 17 and 18, respectively. This is unlike the results found in Figs. 7 and 8 for low-speed driving cycles. During the optimization process, the same GA parameters presented in Table 2 along with the other mentioned assumptions are also considered. From these figures, it was observed that the span of each objective (the difference between the minimum and maximum values) such as T_{Trip}, E, and J_{Avg} in the Pareto fronts are increasing with increasing the trip length.

In the Pareto fronts found in low driving cycles, it was observed that there exist many solutions having a low average jerk value (less than 4 m/s^3) that corresponds to a high trip time and energy consumption or a very high average jerk value (more than 100 m/s^3) with a low trip time and energy consumption. Moreover, by plotting the trip end SOC (SOC) with the T_{Trip} of optimal solutions, even after sorting based on the restricted average jerk values (4 m/s^3 $< J_{\text{Avg}} <$ 100 m/s^3), it was noticed that after a certain trip time there were some solutions in the Pareto-optimal set that possess an uninteresting feature, i.e., the battery SOC is decreasing with increasing trip time. The presence of such uninteresting features was observed for even higher trip lengths, till 10 km. However, for higher trip lengths, the number of such solutions reduces significantly. Such adverse characteristics were not found in the optimal solutions obtained after MOO (multi-objective optimization) for high-speed driving cycles, according to Figs. 17 and 18. Figure 17 and Fig. 18 present the Pareto fronts obtained by the minimization of trip time, energy, and average jerk for a simple micro-tip with different lengths for highway and interstate driving cycles, respectively. Therefore, for high-speed driving cycles, Pareto-optimal solutions after MOO do not require any such sorting based on problem-specific higher level information. The SOC versus T_{Trip} plots are drawn directly after optimization as shown in Figs. 19 and 20 corresponding to the highway and interstate driving cycles, respectively. From

Table 7 Preferred optimal solutions obtained using reference point based method in urban micro-trip

Trip length (km)	Ideal point according to SOC–Time plot	Optimal values of objectives	Optimal values of decision variables					Actual range covered, R
			v	a_k	t_k	k_p	k_i	
0.5	SOC = 0.996379; Time = 35.0901	T_{Trip} = 46.4382; E = 241263; J_{Avg} = 18.4386	55.9811	a_1 = 2.90455; a_2 = 0.196576	t_1 = 2.38019; t_2 = 3.98986	0.206065	1.05836	468.613
5	SOC = 0.968969; Time = 324.565	T_{Trip} = 341.042; E = 1820110; J_{Avg} = 11.9862	55.9898	a_1 = 2.98857; a_2 = 0.145721	t_1 = 2.32508; t_2 = 58.4407	0.156088	0.381912	4972.67

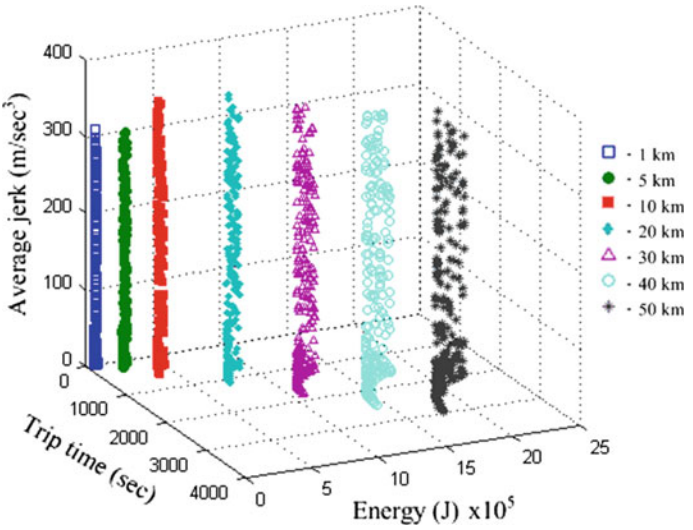

Fig. 17 Pareto-optimal fronts obtained in solving MOOP defined in Sect. 7 in highway driving

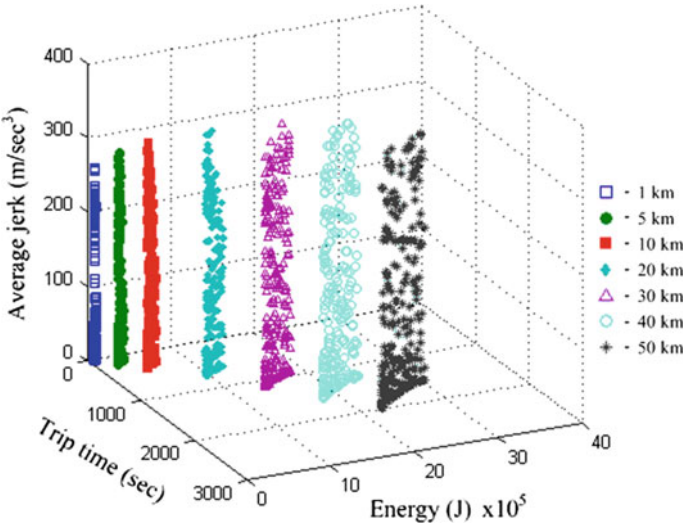

Fig. 18 Pareto-optimal fronts obtained in solving MOOP defined in Sect. 7 in interstate driving

Figs. 19 and 20, it was noticed that the lowest Pareto front *SOC* of any driving cycle is always found to be higher with higher trip length. Contrary to that, the lowest Pareto front trip time of a driving cycle is always noticed to be lower with higher trip length. Such finding is evident since the time requirement and energy consumption are required to be more for a longer trip. This observation suggests the obtained optimization results are meaningful and realistic. In order to demonstrate the optimized

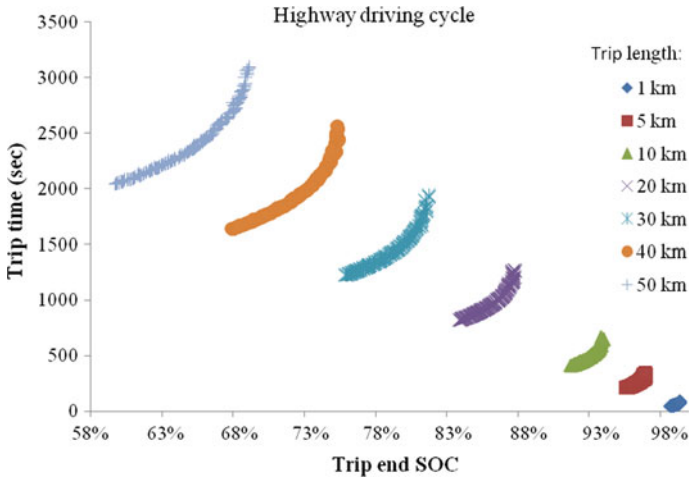

Fig. 19 Variation of trip end SOC with trip time for a highway driving cycle

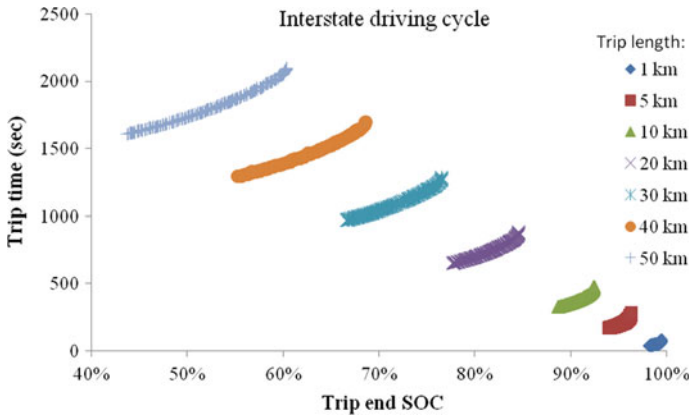

Fig. 20 Variation of trip end SOC with trip time in interstate driving cycle

driving strategy characteristics (*DSC*), a simple micro-trip consisting of one driving cycle (whose velocity profile versus distance is demonstrated in Fig. 6 is considered here. The plots of trip end SOC and trip time for the simple micro-tip of 20 km for highway and interstate driving cycles are shown in Figs. 21 and 22, respectively. Both the figures also demonstrate the corresponding energy consumption, E. The first few best knee-points and the preferred solution obtained using reference point based DM technique are pointed out in the SOC-T_{Trip} plot.

As in low-speed driving cycles, a linear relationship between E and SOC for both highway and interstate driving cycles is found and these are defined in Eqs. (58) and (59), respectively.

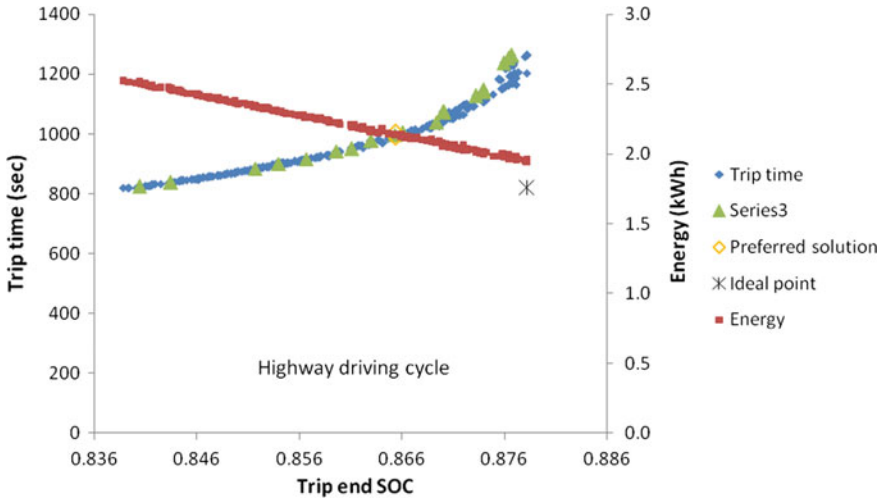

Fig. 21 Energy-trip end SOC–Trip time plot corresponding to minimization of trip time, energy and average jerk in a simple highway micro-tip of 20 km length

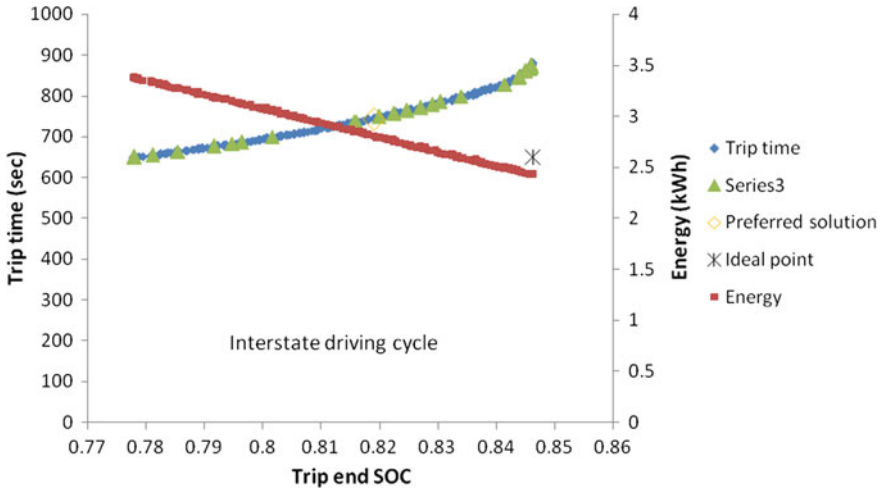

Fig. 22 Energy-trip end SOC–Trip time plot corresponding to minimization of trip time, energy and average jerk in a simple interstate micro-tip of 20 km length

$$E = -14.35SOC + 14.594 \tag{58}$$

$$E = -13.782SOC + 14.164 \tag{59}$$

The slope and intercepts of Eq. (58) are calculated by taking the mean of the slope and intercept values found for different trip lengths in Fig. 17. The corresponding STDs (standard deviations) are 0.198 and 0.215, respectively. Similarly, the slope

and intercepts of Eq. (59) are determined for Fig. 18 and the corresponding STDs are 0.220 and 0.172, respectively. Comparing the relationships between E and SOC for all four driving cycles, it was found that both the slope and intercepts of the linear (average) empirical relation are decreasing with increasing EV speed (v_{ref}). Such findings suggest that in low-speed driving cycles, the SOC decreases with respect to energy consumption at a lower rate compared to that in high-speed driving cycles, which follows typical battery discharge characteristics [4, 61]. This confirms the reliability and meaningful nature of optimization results expected from the proposed DAOTP system.

In Table 8, the values of objective functions (energy consumption, trip time, and average jerk) corresponding to the preferred solutions (representing the optimal driving strategy) obtained through the DAOTP system for high-speed driving cycles for a trip length of 20 km are presented. Table 8 also shows the values of related decision variables (driving characteristics namely EV speed, acceleration(s) and corresponding duration(s), and controller gains), and SOC. Here, two acceleration rates ($k=2$) are assumed during acceleration mode. In contrast to low-speed driving cycles, the optimal speeds were not found to be very close to the upper driving cycle speed limit. Here, it is interesting to note that the optimal speed has a tendency to lie close to the upper driving cycle speed limit as it is varying from high to low. The motivation of such findings can be enlightened by taking into consideration the dependency of motor power and efficiency on speed is explained in [58, 90]. At a low speed, the electric motor efficiency is very low. At medium speeds, it is almost as a constant. At high speeds, the efficiency starts to deteriorate. In order to minimize the trip time, the EV speed is required to be high. Coincidentally, the upper speed limit of a low-speed driving cycle is positioned in the EV speed range that yields the maximum motor efficiency. On the other hand, since power consumption increases in a quadratic manner with EV speed (v) and the maximum speed of a low-speed driving cycle is not too high, MOGA selects the optimal speed closer to the upper limit of the low-speed driving cycle. On the other hand, at high EV speeds, though the trip time reduces, the motor shows low efficiency in addition to the power consumption being extremely high as it is a function of v^2. Therefore, solutions close to the upper limit of the high-speed driving cycle are not selected by MOGA. For these reasons, it is observed that the optimal solution is found further and further away from the upper speed limit of a driving cycle when it changes from low to high speed. As in low-speed driving cycles, a high value of the first acceleration (a_1) is also observed in high-speed driving cycles. On the other hand, for low-speed driving cycles the value of the second acceleration (a_2) was found to be significantly lower than a_1. Though the same result was observed for a highway driving cycles, the a_2 value in the interstate driving cycle was found to be comparatively higher than that in low-speed driving cycles (sometimes, close to a_1). But in those cases, t_2 was found to be opposite in nature. The above findings on optimal DSC are only based on the route characteristic parameters depicted in Table 4. Such findings may be different according to the changes of route characteristic parameters and initial battery SOC. In the following, variations of DAOTP results with these parameters are analyzed for the same trip and driving cycle.

Table 8 List preferred optimal solutions found in different driving cycles for trip length, 20 km

Driving cycle	Ideal point	Optimal values of objectives			Optimal values of decision variables					Trip end SOC	Actual range
		T_{Trip} (s)	E (kWh)	J_{Avg} (m/s^3)	v (km/hr)	a_k (m/s^2)	t_k (s)	k_p	k_i		
Highway	$SOC = 0.878268$; $T_{\text{Trip}} = 818.918$	996.891	2.132308	14.9524	74.0454	$a_1 = 2.49943$; $a_2 = 0.185805$	$t_1 = 3.23687$; $t_2 = 65.8194$	0.201308	0.987817	0.865352	19952.3
Interstate	$SOC = 0.846342$; $T_{\text{Trip}} = 647.571$	743.324	2.807139	21.0881	97.6888	$a_1 = 2.98934$; $a_2 = 2.95014$	$t_1 = 4.05312$; $t_2 = 5.70701$	0.224253	2.91371	0.819008	19926.4

10 Effect of Initial SOC on DAOTP Results

Trip planning is carried out based on the initial battery SOC = 1.0. The EV can attain its maximum range with an optimal driving strategy since the battery energy is maximum. Therefore, a driver can plan a trip with greater confidence, especially if the trip length is below the maximum range. In certain situations, a full battery SOC before starting a trip may not be possible. Besides this, the study of the effect of initial SOC on DAOTP results [52] is important in the sense that if the vehicle is unexpectedly required to stop or to modify the original trip plan or due to some unforeseen reason, the original DAOTP results may no longer be valid. In that case, the remainder of the trip must be planned once more based on the current SOC, which would be different from the initial SOC before the trip was initiated. This scenario is not to be confused with the general operation of DAOTP, which continuously updates itself. That is, once the trip is planned, DAOTP updates itself after each time interval, but the optimal driving strategy remains the same provided the route characteristics also remain the same.

The battery energy depleted in terms of SOC difference between before and after the trip performed is presented in Figs. 23 and 24 in highway and interstate driving cycles, respectively. The results are taken considering a trip length of 20 km. From both the figures, it was observed that the rate of decreasing *SOC* is more when the initial battery SOC is low compare to high initial SOC irrespective of driving cycle type. For instance, to complete the 20 km interstate trip in 800 s, the SOC drops are found to be 44.565%, 29.288%, 21.356%, and 16.480% corresponding to the initial battery SOCs 0.4, 0.6, 0.8 and 1.0, respectively as found in Fig. 24. Considering the same trip length and initial SOC values (0.4, 0.6, 0.8 and 1.0), the SOC drops are found as 39.47%, 25.825%, 18.96, and 14.54%, respectively, for a highway for a trip time of 900 s, as shown in Fig. 23. These results offer the conclusion that *SOC* significantly depends on the initial battery SOC. The amount of *SOC* dropped with initial battery SOC follows an intricate relationship which is not studied here. Moreover, a unique relationship does not exist for all driving cycles. The width of the Pareto-optimal front corresponding to both *SOC* and trip time in a driving cycle does vary with the initial SOC value. Figures 23 and 24 also show the distance (range) covered by EV with initial SOC = 0.4. It is observed that all the solutions in the Pareto front are found to cover the 20 km trip length for a highway driving cycle. However, for the interstate driving cycle, some solutions are found that are not able to complete the entire trip. The SOC values of those solutions with trip time less than 600 min decrease below the limiting SOC value of 0.2 (a typical value to protect the battery and it offers a safety factor) before completing the desired trip length of 20 km. The above findings argued that an averaging method (a naive predictor) on the basis of previous experiences of past trip may suggest incorrect results where SOC consumption in concerned, specifically if it is a different driving cycle type. For most of the cases, the initial SOC of the present trip may not be the same as adopted in the previous trip. Moreover, changing the route characteristic information increases the

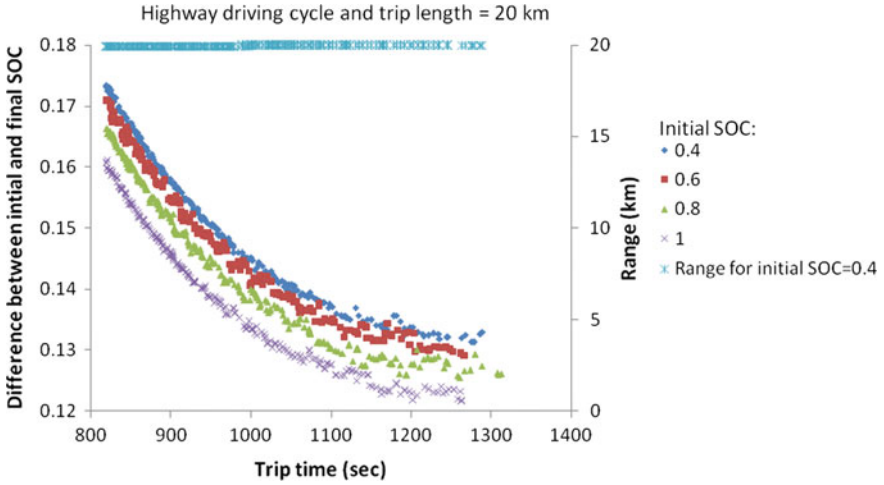

Fig. 23 SOC change with trip time for a highway driving cycle

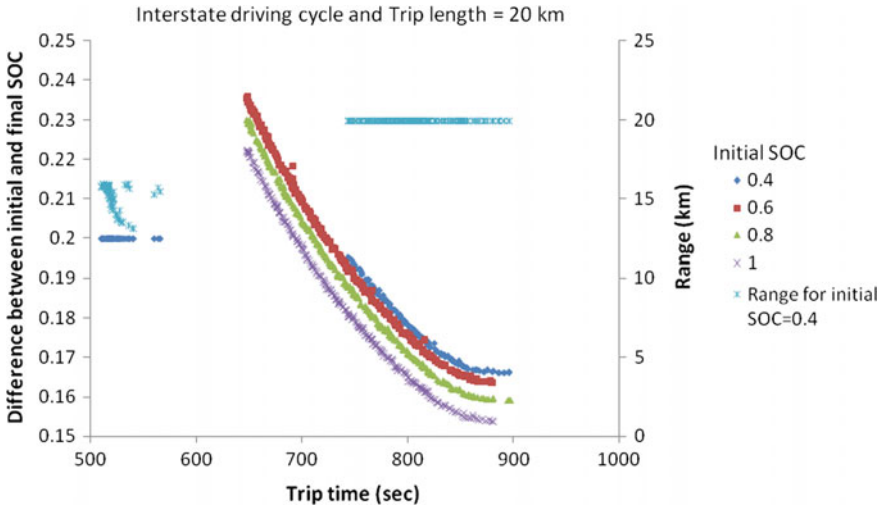

Fig. 24 SOC change with trip time in interstate driving cycle

probability of yielding inaccurate trip planning results. These issues are discussed in the subsequent section.

Table 9 Road gradient distribution of the micro-trip route

Sr. No.	Distance (km)		Gradient
	From	To	
1	0	2	0
2	2	8	Gradient value
3	8	12	0
4	12	18	−Gradient value
5	18	20	0

11 Influence of Route Characteristics on DAOTP Results

The influences of various route characteristic parameters on the DAOTP results are presented here [52]. Among various route characteristic parameters, the present study considers the most influential and common ones. These are the road gradient, wind velocity and direction, road surface, and air density due to change of elevation.

11.1 Road Gradient

In order to investigate the road gradient influence on DAOTP results, eight different road gradient values ranging from 0 to 3° are taken. The route architecture corresponding to each micro-trip follows the road gradient distribution presented in Table 9. Each route consists of both road gradient effects that may be encountered during a trip, uphill and downhill, denoted by positive and negative signs, respectively, in Table 9. Each gradient zone extends for an equal length, 6 km, in the trip. This is representative of a round trip, wherein the driver ends up at the starting point after trip, meaning there is no net change in elevation due to the road gradient.

Figure 25a, b demonstrate the influence of road gradients on DAOTP outcomes for highway and interstate driving cycles, respectively. It is quite obvious that more energy is consumed to maintain a constant vehicle speed in a road with positive gradient. In contrast, braking may be required in a road with negative gradient to keep a constant speed. However, during braking, there is a scope to recover the EV kinetic energy to some extent through regeneration techniques. The energy recuperation efficiency of a regenerative braking system depends on many factors such as vehicle speed, battery SOC, battery temperature, motor available braking torque, braking force, braking behavior [37], etc. and has a complex nature [43]. In the present study, the regenerative braking factor, *Regen* (defined by the fraction of the total available regenerative energy that is converted to battery energy), is considered as 0.5, which is a typical value for EVs. The deceleration rate is considered according to the vehicle speed defined in Eq. (51).

Although the positive and negative road gradient exist for the same fraction of the trip, the DAOTP results with the road gradient effect are found to be different

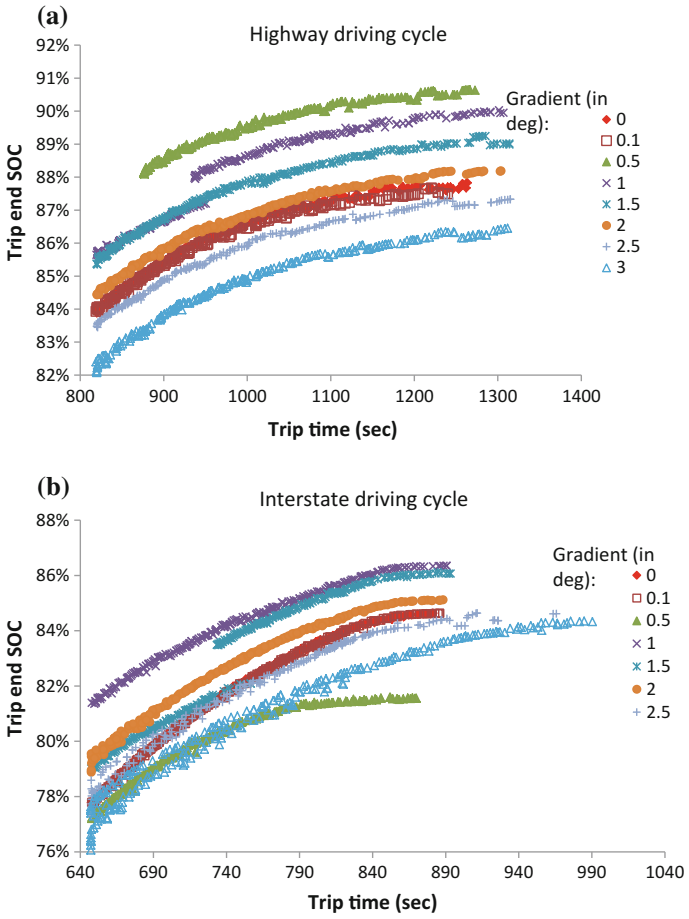

Fig. 25 Variation of trip end SOC with trip time for different road gradients to cover a trip length of 20 km in **a** Highway and **b** Interstate driving cycles

from that with zero gradient for both the driving cycles. For the highway driving cycle, a small gradient ($\leq 2°$) improves the trip end SOC, except very small gradient (0.1) or without any gradient. For high gradients ($>2°$), the trip end SOC deteriorates significantly, meaning more energy consumption during positive gradient than energy recovery through regeneration during negative gradient. These results highly depend on the regenerative braking system used and road gradient distribution of the rout. The influence of road gradient on network-wide vehicle energy consumption can be found in [59]. The same effects on the DAOTP results with road gradient were found for the interstate driving cycle. However, the Pareto front characteristic corresponding to different road gradient with respect to that of zero road gradient is not similar for highway and interstate driving cycles.

11.2 Wind Speed and Its Direction

In order to demonstrate the wind effect on DAOTP results, two wind speeds (10 and 30 km/h) blowing in two different directions (0° and 135° with respect to the EV driving direction) are considered. The results obtained with wind are compared with those obtained without wind. The Pareto fronts are presented in Fig. 26a, b. Figure 26a, b show the comparative results for highway and interstate driving cycles, respectively.

Generally, an energy saving is anticipated when the wind blowing in the direction of vehicle speed. In contrast, high energy consumption is needed while the wind flow is against the vehicle speed. A similar notion is also observed in the results presented in Fig. 26. However, the effect of wind on energy consumption variations follows a complex relationship. Various parameters such as vehicle speed, wind speed, and its direction, vehicle driving modes, etc. have an effect on the energy consumption. After analyzing the results, it was observed improvement rate of energy consumption is comparatively less than the deterioration rate of that. The reason behind such kind of phenomenon is that drag force is proportional to the squared of vehicle effective speed, as shown in Eq. (35). However, an unexpected observation for highway driving cycles was noticed in the case when the wind is in the same direction as the vehicle, as shown in Fig. 26a. It was noticed that some solutions in the Pareto front, particularly those having a high trip time, exhibit a trip end SOC that is less than that found without any wind. Moreover, as the wind speed increases, more solutions are found to follow this behavior. Through further simulations (not presented in this chapter), it was found that when the wind speed is very high (>50 km/h), the solutions follow the behavior as observed in Fig. 26b. Similar findings were noticed in low-speed driving cycles. The reason may be due to the fact that wind in the same direction as the vehicle speed reduces the net drag force. As a result, it accelerates the vehicle more per unit time step which yields more jerk. In the present MOOP, one of the objectives is to minimize the average jerk (calculated using Eq. (48)), so MOGA does not select those solutions experiencing more jerk. In low-speed driving cycles (low v_{ref}), the acceleration duration is shorter than that in high-speed driving cycles and a short acceleration duration yields a comparatively a high average jerk. For this reason, such results are observed in the optimal solutions when applying the DAOTP system to low-speed driving cycles.

Practically, wind follows a turbulent behavior in on-road environment. Due to that the wind effect on energy consumption becomes complicated in nature [97]. Thus, the nature of the results considering wind turbulence effects is difficult to predict [21, 98].

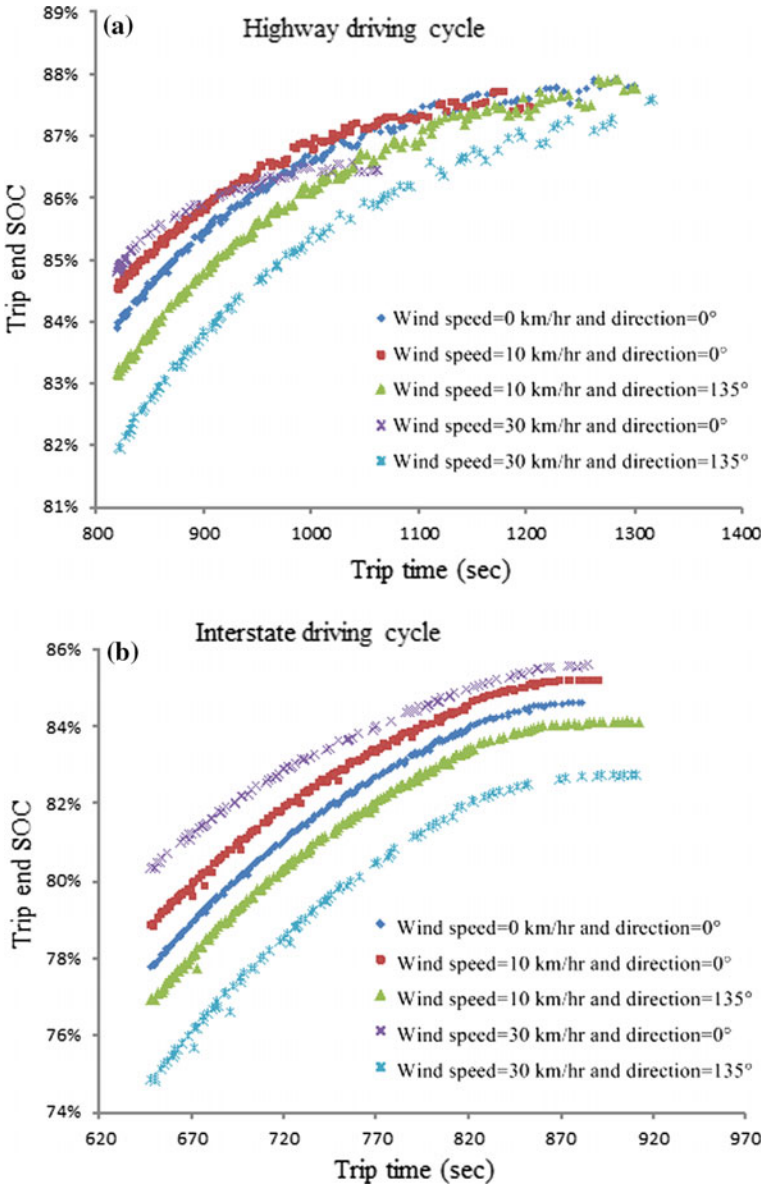

Fig. 26 Effect of wind on DAOTP results to cover a trip length of 20 km in **a** Highway and **b** Interstate driving cycles

Table 10 Road surface rolling frictional coefficient distribution of the micro-trip route

Sr. No.	Distance (km)		Friction coefficient of road surface
	From	To	
1	0	10	0.015
2	10	20	*M*

11.3 Road Surface

The properties of the road surface that affect the objectives, trip time, energy consumption, and jerk, are surface irregularity and rolling friction coefficient, μ [48]. So far, the above studies were carried out for a constant road surface with $\mu = 0.015$. The factor, irregularity, particularly restricts the speed limit of a route with the goal of avoiding jerk and accidents. This results in affecting the vehicle energy consumption. The effect of this factor can be simply tackled by constraining the speed limit of a route before finding optimum driving strategy. Thus, the influence of road surface irregularity on the DAOTP results is not investigated here. The effect of the rolling friction coefficient on the DAOTP results is investigated by comparing the *SOC* with respect to trip time plot found for six different friction coefficients. This study is carried out with a micro-trip of length 20 km having the first 10 km length with $\mu = 0.015$ and the remaining 10 km length with a different μ value, as shown in Table 10. Figure 27a, b demonstrate *SOC* with the trip end time for highway and interstate driving cycles, respectively, for different μ values. From these figures, it was noticed that *SOC* was found to be reduced as rolling frictional coefficient increases. Furthermore, it was noticed that for low value of μ (0.015), a little increase in μ results to a high loss of *SOC*. But, when μ is 0.02 or above, a uniform loss of *SOC* with increasing μ was found.

The friction coefficient between the tire and the roadway depends on the material used to make the road (such as asphalt, basalt, concrete, epoxy, etc.), the road surface condition (such as dry, wet, etc.), and the natural deterioration of the road surface roughness due to traffic and climate [47]. There are well-established methods to measure the road surface friction coefficients [1]. A detailed study on vehicle fuel consumption due to friction resistance can be found in [70]. These studies are applicable for any vehicle type.

11.4 Elevation

The elevation primarily affects the temperature and pressure of air at that location. This results in changing the air density thereby affecting the drag force acting on the EV. A high elevation with respect to sea level decreases the air density. The above studies were carried out for a constant air density, $\rho_{air} = 1.143$ kg/m^3. In

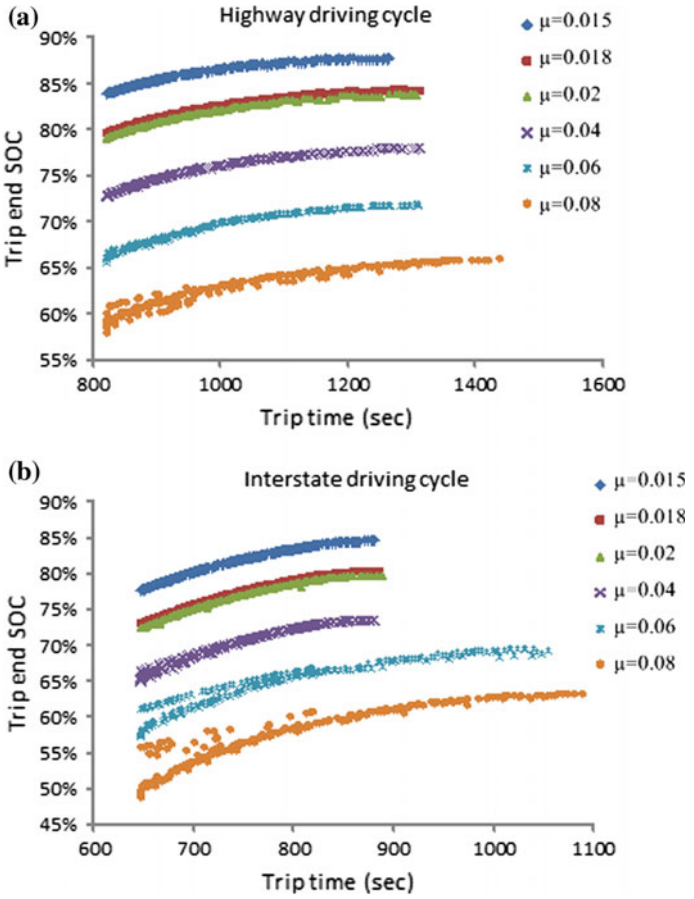

Fig. 27 Effect of road rolling friction coefficient on DAOTP results to cover a trip length of 20 km for **a** Highway and **b** Interstate driving cycles

order to analyze the effect of air density on the DAOTP results, a micro-trip is considered where the ρ_{air} of a part of the route is varied, as shown in Table 11. In order to understand the effect of road elevation only, the road gradient is assumed here constant, though normally in a trip, the elevation effect is always present in association with road gradient. The results for three air density values are presented in Fig. 28a, b for highway and interstate driving cycles, respectively. In both high-speed driving cycles, an improvement in trip end SOC was observed by reducing the air density. The effect of air density was not found to be more significant comparing to other route parameters.

As the elevation increases, the air becomes thinner. Since air is needed for combustion, and due to the unavailability of air at higher altitudes, diesel engine produces a lesser amount of power. For, In high altitude in theory gasoline engines requires less

Table 11 Air density distribution of the micro-trip route

Sr. No.	Distance (km)		Density of air (due to elevation)
	From	To	
1	0	2	1.143
2	2	18	ρ_{air}
3	18	20	1.143

fuel due to lower throttle friction from wider throttle opening. In [103], a study on fuel consumption due to the impact of elevation of a gasoline passenger car was carried out. It was found that the reduction of energy consumption was different in different driving cycles and different elevations. Moreover, the impact of higher elevation was not apparent and there is not always a decrease in fuel consumption, as also observed in Fig. 28a. Interestingly enough, EVs (powered by batteries and electric motors) are nearly immune to power losses due to elevation in this respect. Moreover, as air gets thinner at higher altitude, the drag force reduces, and corresponding the energy consumption.

12 Influence of Micro-trip Complexity on DAOTP Results

A complex micro-trip is defined as a micro-trip consisting of two or more driving cycles. Here, the DAOTP results are investigated for a complex micro-trip that consists of two neighborhood portions and one highway portion. The influence of micro-trip complexity on DAOTP results are analyzed by comparing the trip end SOC versus trip time of optimal solutions from a complex micro-trip with those found in simple micro-trip consisting of either a neighborhood or a highway driving cycle. The positions and lengths of the different portions are shown in Table 12, keeping the total trip length at 20 km. Figure 29 presents the demonstrative DAOTP results for the different complex micro-trips. These are formulated by considering different lengths of the highway portion in order to know how complex micro-trip results vary with composition. In the Fig. 29 legend, the first and last entries correspond to purely neighborhood and purely highway micro-trips, respectively, based on the formulas used in Table 12. From Fig. 29, it was found that as the length of the highway portion increases, the Pareto front width in terms of both objectives is expanded. The trip end SOC is found to be increasing in both directions whereas the trip time always decreasing as the highway portion's length increases. Using the ideal point based reference point technique of a finding preferred solution, the optimal trip end SOC are 0.855346, 0.856298, 0.858101, 0.863259, and 0.865352 for highway driving cycle lengths 0, 5, 10, 15, and 20 km, respectively. There is a polynomial relationship observed between the trip end SOC and the highway portion length. Such a relationship is not applicable to any kind of complex micro-trip. Practically,

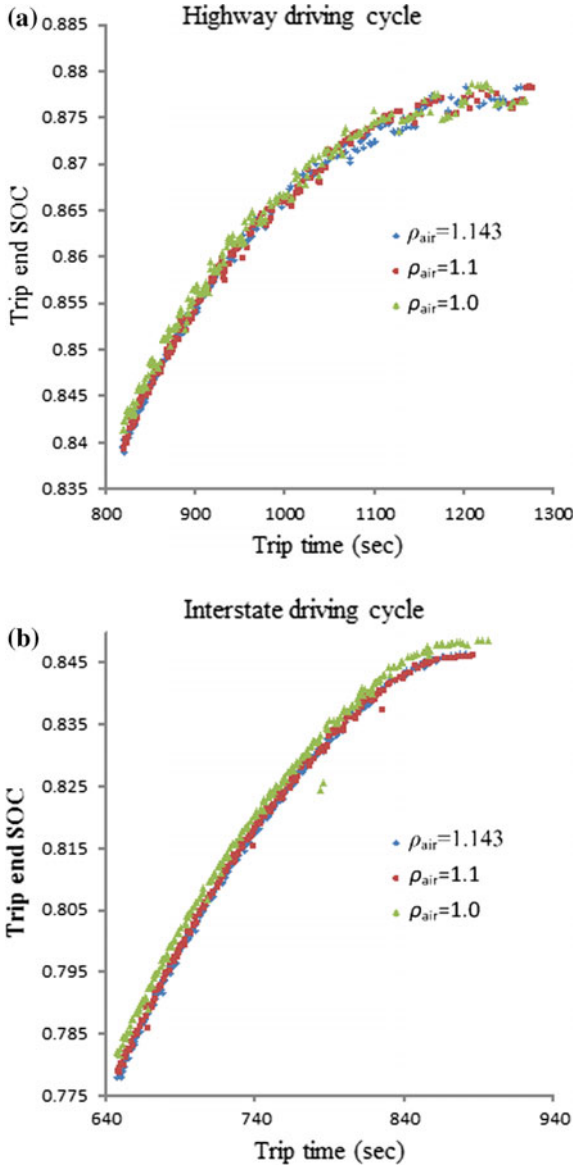

Fig. 28 Effect of air density on DAOTP results to cover a trip length of 20 km in **a** Highway and **b** Interstate driving cycles

depending on the complexity, the types of driving cycle involved, their lengths, and their positions in the micro-trip, this relationship changes.

The DAOTP system presented in this chapter directs the driver not only for proper driving but also it allows the EV to function each components efficiently with their highest efficiency level. Consequently, it lowers the energy consumption and enhances the service life of EV components and safety as well. Thereby, EV

Table 12 Architecture of complex trip

Sr. No.	Micro-trip distance (km)		Driving cycle
	From	To	
1	0	(Total trip length − Length of highway)/2	Neighborhood
2	(Total trip length − Length of highway)/2	Length of highway	Highway
3	(Total trip length − Length of highway)/2	Total trip length	Neighborhood

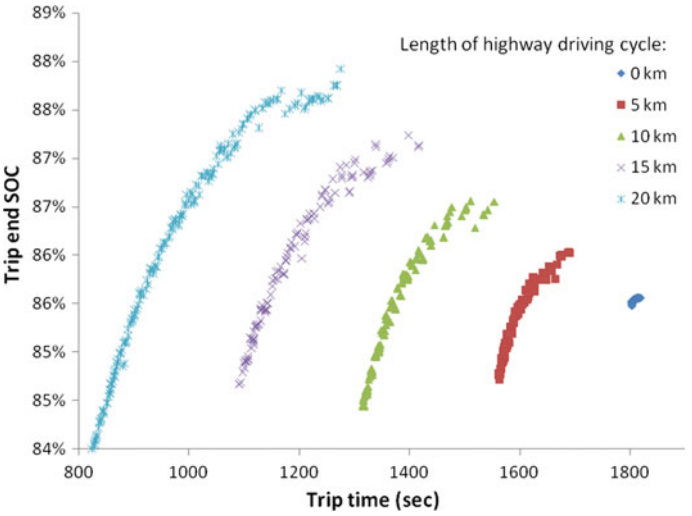

Fig. 29 Variation of trip end SOC with trip time for different complex micro-trips

operating costs becomes reduced. Moreover, the overall driving experience is also improved by adopting the assistances offered by DATOP system. Present driver assistance systems (DAS) may offer useful energy utilization for EVs through finding a low cost path to the destination but they do not assist the driver how to operate the EV components competently. The most significant benefit of DAOTP compared to existing ADAS is that it assists the driver by supporting an optimal driving strategy to follow throughout the entire trip. By doing so, it can guarantee the trip completion without of the possibility of exhausting the battery energy unexpectedly before the trip is completed. Otherwise, it gives a caution prior to the trip or well before the complete battery charge depleted to a take an alternative decision such as to find a charging station. Consequently, a high level of assurance towards successfully performing the trip is built up in driver's mind. Thus, use of DAOTP certainly promotes the popularization of environmentally friendly EVs by growing the reliability of EVs in the public's perception, which is not found so far.

In the present article, jerk that hinders the comfortable journey is assumed to be generated due to changes of acceleration/deceleration rate. Besides this, there are other causes of experiencing jerk, such as driveline dynamics, indiscretion of road, variation of wind speed, etc. that are not considered here. Jerk generated due to such causes may be minimized by taking precautions such as restricting the speed limit, etc. The proposed DAOTP can be integrated with existing DAS such as AHS (Automated Highway Systems), ADAS (Advanced Driver Assistance System), Navigation and Routing devices [102], etc.

13 Summary and Conclusions

A novel and easy to implement driving assistance strategy for EVs, DAOTP is presented here. The proposed DAOTP approach is unique and is superior to existing methods because of its multi-faceted approach. It is model-specific, which means it considers all the characteristics of the vehicle in question and ensures that the hardware such as the electric motor is operated in the most efficient regime. If there are conflicts amongst different hardware regimes, the algorithm chooses a globally optimal solution on the basis of efficiency trade-offs amongst all the hardware involved. This means that the stored energy is used in an efficient manner making DAOTP an energy management strategy as well. The key feature of DAOTP is trip planning: providing the driver with several optimal driving strategies to negotiate a trip so as to optimize various conflicting objectives such as minimum discomfort, energy consumption, and time. Not only does this provides an efficient and comfortable ride, but also instills some measure of confidence in the driver that the EV will be able to reach the destination given the current SOC status. The multi-objective approach gives the driver the ultimate freedom to decide which objectives are more important. This choice is bound to vary from driver to driver and DAOTP takes this into consideration. Finally, DAOTP is an online system, which means not only does it give the driver prior knowledge about the driving strategy for a given trip, it also updates itself based on current road and trip conditions, some of which may be unforeseen. The result is that the driver always has knowledge of the optimal driving strategy for the remainder of the trip, which may be different from the first predicted driving strategy prior to the commencement of the trip.

In the present chapter, the proposed DAOTP architecture for an EV and the role of each component associated with this system are described. The DAOTP executes by solving a multi-objective optimization problem involving minimizations of trip time, energy consumption, and average jerk. The models of these objectives are presented considering the three EV components, battery, electric motor, and vehicle dynamics. A multi-objective genetic algorithm is utilized to solve the multi-objective problem. The DAOTP system is applied first in low-speed driving cycles considering a simple micro-trip. Trip planning, starting from identifying a route based on trip starting point and destination, how to receive the route characteristic data through HMI using GPS and Internet, utilizing these data, producing a set of Pareto-optimal solution after

solving the multi-objective problem, then identifying the set of interesting solutions based on a sorting process using problem-specific information, and finally selecting a preferred solution based on a decision-making technique or driver's choice for implementation, is systematically presented. It has been observed that an optimized driving strategy may substantially reduce EV energy consumption. Analyzing DAOTP results for low-speed driving cycles in different trip lengths clearly indicates its importance for implementation in EV.

The results of the DAOTP system for a micro-trip in high-speed driving cycles were presented later. The optimal driving strategies were determined through a multi-objective optimization of minimizing total trip time, energy consumption, and the average jerk during speed changing. The influence of various route parameters and the initial SOC on the DAOTP results were investigated through the analysis of the trip end SOC with respect to the trip time of the optimal solutions obtained after the optimization process.

Effects of *initial battery SOC*, wind, road gradient and elevation on energy consumption, trip time and jerk are carried out here, and the research findings suggest that based on the naïve predictors that use previous trip performing experience planning of current trips may not be an optimum one. Moreover, naïve predictors are unable to provide energy-driving parameters. The present DAOTP systems considers the route characteristics and driver's preference while providing an optimal driving strategy that leads to an energy-efficient trip with minimum trip time and discomfort. Extensive analysis of the results suggests that the proposed approach is reliable as well as efficient. It is concluded that approaches based on previous experience is not sufficient for EV trip planning, and the present DAOTP system is a substitute to address this necessitate.

Acknowledgements This book chapter is written based on the partial research work carried out under Indo-US fellowship program (Fellowship Letter Reference: IUSSTF Fellowships 2013/14) supported by IUSSTF, India.

References

1. Ahn, C., Peng, H., & Tseng, H. E. (2013). Robust estimation of road frictional coefficient. *IEEE Transactions on Control Systems Technology, 21*(1), 1–13.
2. Ameratunga, S. (2009). Traffic speed zones and road injuries: Speed management is key. *BMJ, 339,* b4743. https://doi.org/10.1136/bmj.b4743.
3. Andre, M. (2004). *Real-world driving cycles for measuring cars pollutant emissions—Part A: The ARTEMIS European driving cycles*. Institut National de Recherche sur les Transports et leur Securite (INRETS), Report INRETS-LTE 0411.
4. Andrea, D. (2010). *Battery management systems for large lithium ion battery packs*. Artech House Publishers.
5. Alfraheed, M., Dröge, A., Klingender, M., Schilberg, D., & Jeschke, S. (2011). Longitudinal and lateral control in automated highway systems: Their Past, present and future. In S. Jeschke, H. Liu, & D. Schilberg (Eds.), *ICIRA 2011, Part II, LNAI 7102* (pp. 589–598). Berlin, Heidelberg: Springer.

6. Baronti, F., Zamboni, W., Femia, N., Saletti, R., & Chow, M. Y. (2013). Parameter identification of Li-Po batteries in electric vehicles: A comparative study. In *IEEE International Symposium on Industrial Electronics*, Taipei, Taiwan, May 28–31, 2013 (pp. 1–7). https://doi.org/10.1109/isie.2013.6563887.
7. Bergenhem, C., Hedin, E., & Skarin, D. (2012). Vehicle-to-vehicle communication for a platooning system. *Procedia—Social and Behavioral Sciences, 48,* 1222–1233.
8. Berry, M. I. (2010). *The effects of driving style and vehicle performance on the real-world fuel consumption of US light-duty vehicles*. Master's Thesis, Massachusetts Institute of Technology. http://web.mit.edu/sloan-auto-lab/research/beforeh2/files/IreneBerry_Thesis_February2010.pdf.
9. Bingham, C., Walsh, C., & Carroll, S. (2012). Impact of driving characteristics on electric vehicle energy consumption and range. *IET Intelligent Transport Systems, 6*(1), 29–35.
10. Bodin, L., & Levy, L. (1994). Visualization in vehicle routing and scheduling problems. *ORSA (Operation Research Society of America) Journal on Computing, 6*(3), 281–288.
11. Branke, J., Deb, K., Dierolf, H., & Osswald, M. (2004). Finding knees in multi-objective optimization. In X. Yao et al. (Eds.), *PPSN 2004*. LNCS 3242 (pp. 722–731). Heidelberg: Springer.
12. Cai, L., Rad, A. B., & Chan, W. L. (2007). A genetic fuzzy controller for vehicle automatic steering control. *IEEE Transactions on Vehicular Technology, 56*(2), 529–543.
13. Carminat Tom Tom Navigation System [CTTNS]. (2012). Retrieved December, 2014, from http://www.tomtom.com/en_gb/products/built-in-car-navigation/carminat-tomtom/.
14. Ceraolo, M., & Pede, G. (2001). Techniques for estimating the residual range of an electric vehicle. *IEEE Transactions on Vehicular Technology, 50*(1), 109–115.
15. Chakraborty, D., & Nandi, A. K. (2016). Finding optimal deceleration with serial regenerative braking of electric vehicle using a multi-objective genetic algorithm. In *IEEE International Conference on Power Electronics, Intelligent Control and Energy Systems (IEEE ICPEICES 2016)*, Delhi, India, July 4–6, 2016. https://doi.org/10.1109/icpeices.2016.7853333.
16. Chakraborty, D., & Nandi, A. K. (2016). Finding optimal driving strategy zone of electric vehicle during deceleration with serial regenerative braking. In *7th Power India International Conference (IEEE PIICON 2016)*, Rajasthan, India, November 25–27, 2016.
17. Chale-Gongora, H. G., de Weck, O., Doufene, A., Ishimatsu, T., & Krob, D. (2014). Planning an itinerary for an electric vehicle. In *Proceedings of IEEE Energy Conference (ENERGYCON 2014)*, Cavtat, Dubrovnik, Croatia, May 13–16, 2014 (pp. 1385–1391).
18. Cheng, C., McGordon, A., Poxon, J., Jones, R., & Jennings, P. (2010). A model to investigate the effects of driver behaviour on hybrid vehicle control. In *25th World Battery, Hybrid, and Fuel Cell Electric Vehicle Symposium and Exhibition*, Shenzhen, China, November 5–9, 2010.
19. Chen, M., & Rincón-Mora, G. A. (2006). Accurate electrical battery model capable of predicting runtime and I–V performance. *IEEE Transactions on Energy Conversion, 21*(2), 504–511.
20. Chen, Y. L., Huang, C. H., Kuo, Y. W., & Wang, S. S. (2012). Artificial neural network for predictions of vehicle drivable range and period. In *Proceeding of IEEE International Conference on Vehicular Electronics and Safety*, Istanbul, Turkey, July 24–27, 2012 (pp. 329–333).
21. Cooper, K. R., & Watkins, S. (2007). *The unsteady wind environment of road vehicles, Part One: A review of the on-road turbulent wind environment*. SAE Technical Paper 2007-01-1236.
22. Cortes, P., Larraneta, J., Onieva, L., Garcia, J. M., & Caraballo, M. S. (2001). Genetic algorithm for planning cable telecommunication networks. *Applied Soft Computing, 1*(1), 21–23.
23. Deb, K. (2000). An efficient constraint handling method for genetic algorithms. *Computer Methods in Applied Mechanics and Engineering, 186*(2/4), 311–338.
24. Deb, K., Pratap, A., Agarwal, S., & Meyarivan, T. (2002). A fast elitist non-dominated sorting genetic algorithm for multi-objective optimisation: NSGA-II. *IEEE Transactions on Evolutionary Computation, 6*(2), 182–197.
25. Demestichas, K., Adamopoulou, E., Kipp, W., Kaminski, T., & Benz, T. (2011). EcoGem: An intelligent advanced driver assistance system for fully electric vehicles. In *18th World Congress on Intelligent Transport Systems*, Orlando, Florida, U.S.A., October 16–20, 2011.

26. Demestichas, K., Adamopoulou, E., Masikos, M., Kipp, W., & Benz, T. (2011). Intelligent advanced driver assistance system for electric vehicles. In *IEEE Intelligent Vehicles Symposium (IV)*, Baden-Baden, Germany, June 5–9, 2011 (pp. 78–82).
27. Dib, W., Serrao, L., & Sciarretta, A. (2011). Optimal control to minimize trip time and energy consumption in electric vehicles. In IEEE *Conference on Vehicle Power and Propulsion Conference (VPPC)*, Chicago, IL, September 6–9, 2011 (pp. 1–8). https://doi.org/10.1109/vppc.2011.6043133.
28. Dovgan, E., Tušar, T., Javorski, M., & Filipič, B. (2012). Discovering comfortable driving strategies using simulation-based multiobjective optimization. *Informatica (Slovenia), 36*(3), 319–326.
29. Du, L. L., Li, B., & Zhang, H. D. (2013). Estimation on state of charge of power battery based on the grey neural network model. *Applied Mechanics and Materials, 427–429,* 1158–1162.
30. Eisner, J., Funke, S., & Storandt, S. (2011). Optimal route planning for electric vehicles in large networks. In *Proceedings of the Twenty-Fifth AAAI Conference on Artificial Intelligence*, Hyatt Regency San Francisco, August 7–11, 2011 (pp. 1108–1113).
31. Fambro, D. B., Fitzpatrick, K., & Koppa, R. J. (1997). *Determination of stopping sight distance*. NCHRP (National Cooperative Highway Research Program) Report 400, National Academy Press, Washington D.C.
32. Feng, L., Ge, S., & Liu, H. (2012). Electric vehicle charging station planning based on weighted Voronoi diagram. In *Proceedings of Power and Energy Engineering Conference (APPEEC), 2012 Asia-Pacific*, March 27–29, 2012 (pp. 1–5). IEEE.
33. Fiat Eco: Drive, Eco-driving uncovered: the benefits and challenges of eco-driving based on the first study using real journey data (2010). Retrieved February 10, 2015, from http://www.lowcvp.org.uk/assets/reports/Fiat_Eco-Driving%20Uncovered.pdf.
34. Franke, T., Neumann, I., Bühler, F., Cocron, P., & Krems, J. F. (2012). Experiencing range in an electric vehicle: Understanding psychological barriers. *Applied Psychology: An International Review, 61*(3), 368–391.
35. Fujii, H., Hayashi, O., & Nakagata, N. (1996). Experimental research on intervehicle communication using infrared rays. In *Proceedings of IEEE Intelligent Vehicles Symposium*, Tokyo, Japan, September 19–20, 1996 (pp. 266–271).
36. Gantt, L. R., Alley, R. J., & Nelson, D. J. (2011). Battery sizing as a function of powertrain component efficiencies for various drive cycles. In *ASME International Design Engineering Technical Conferences & Computers and Information in Engineering Conference (IDETC/CIE 2011)*, August 28–31, 2011, Washington, DC.
37. Gao, Y., Chen, L., & Ehsani, M. (1999). *Investigation of the effectiveness of regenerative braking for EV and HEV*. SAE Technical Paper 1999-01-2910. https://doi.org/10.4271/1999-01-2910.
38. Garmin ecoRoute HD software [GEHDS]. (2010). Retrieved January, 2015, from http://www.garmin.com.
39. Ghoseiri, K., & Ghannadpour, S. F. (2010). Multi-objective vehicle routing problem with time windows using goal programming and genetic algorithm. *Applied Soft Computing, 10*(4), 1096–1107.
40. Gillespie, T. D. (2003). *Fundamentals of vehicle dynamics*. Society of Automotive Engineers, Inc. 400 Commonwealth Drive, Warrendale, PA 15096-0001.
41. Global Positioning System, Volume 1—Theory and Applications [GPSTA]. (1996). In B. Parkinson, J. Spilker, P. Axelrad & P. Enge (Eds.), Published by the American Institute of Aeronautics and Astronautics, Inc. 370 L'Enfant Promenade, SW, Washington, DC 20024-2518. ISBN 978-1-56347-106-3.
42. Grant, P. R., & Haycock, B. (2008). Effect of jerk and acceleration on the perception of motion strength. *Journal of Aircraft, 45*(4), 1190–1197.
43. Guo, J., Wang, J., & Cao, B. (2009). Regenerative braking strategy for electric vehicles. In *IEEE Conference on Intelligent Vehicles Symposium*, June 3–5, 2009, Xi'an, China (pp. 864–868).

44. Haan, P. D., & Keller, M. (2001). *Real-world driving cycles for emission measurement: ARTEMIS and Swiss cycles*. Final Report.
45. Harding, J., Powell, R. G., Yoon, R., Fikentscher, J., Doyle, C., Sade, D., et al. (2014). *Vehicle-to-vehicle communications: Readiness of V2V technology for application*. Washington, DC: National Highway Traffic Safety Administration, Report No. DOT HS 812 014.
46. Hansen, T., & Wang, C.-J. (2005). Support vector based battery state of charge estimator. *Journal of Power Sources, 141*(2), 351–358.
47. Heissing, B., & Ersoy, M. (2011). *Chassis handbook fundamentals, driving dynamics, components, mechatronics, perspectives*. Wiesbaden: Vieweg + Teubner Verlag | Springer Fachmedien Wiesbaden GmbH.
48. ID4EV project [ID4EVP]. (2014). Retrieved December, 2014, from http://www.id4ev.eu.
49. Imanishi, H., Takada, Y., & Wakisaka, T. (2002). An acceleration control algorithm for an electric motor driven vehicle in consideration of the reduction of energy consumption. *Nippon Kikai Gakkai Ronbunshu, C Hen/Transactions of the Japan Society of Mechanical Engineers, Part C, 68*(5), 1512–1517.
50. Ishimatsu, T., de Weck, O., Hoffman, J., Ohkami, Y., & Shishko, R. (2013). A generalized multi-commodity network flow model for space exploration logistics. In *AIAA SPACE 2013 Conference & Exposition*, San Diego, California, USA, September 10–12, 2013.
51. Karmakar, M., & Nandi, A. K. (2016). Trip planning for electric vehicle through optimal driving using genetic algorithm. In *International Conference on Power Electronics, Intelligent Control and Energy Systems (IEEE ICPEICES 2016)*, July 4–6, 2016, Delhi, India.
52. Karmakar, M., & Nandi, A. K. (2016). Driving assistance for energy management in electric vehicle. In *International Conference on Power Electronics, Drives and Energy Systems (IEEE PEDES 2016)*, December 14–17, 2016, Trivandrum, India.
53. Kato, S., Tsugawa, S., Tokuda, K., Matsui, T., & Fujii, H. (2002). Vehicle control algorithms for cooperative driving with automated vehicles and intervehicle communications. *IEEE Transactions on Intelligent Transportation Systems, 3*(3), 155–161.
54. Kim, E., Lee, J., & Shin, K. G. (2013). Real-time prediction of battery power requirements for electric vehicles. In *Proceeding of ACM/IEEE International Conference on Cyber-Physical Systems*, Philadelphia, PA, USA, April 8–11, 2013 (pp. 11–20).
55. Knowles, M., Scott, H., & Baglee, D. (2012). The effect of driving style on electric vehicle performance, economy, and perception. *Int. J. of Hybrid Vehicles, 4*(3), 228–247.
56. Kockelman, K. (2006). *Safety impacts and other implications of raised speed limits on high-speed roads*. NCHRP (National Cooperative Highway Research Program) Web-Only Document 90 (Project 17-23): Contractor's Final Report, Transportation Research Board of the National Academies.
57. Kunze, R., Ramakers, R., Henning, K., & Jeschke, S. (2009). Organization and operation of electronically coupled truck platoons on German motorways. In M. Xie, Y. Xiong, C. Xiong, H. Liu, & Z. Hu (Eds.), *ICIRA 2009*. LNCS-5928. Heidelberg: Springer (pp. 135–146).
58. Larminie, J., & Lowry, J. (2012). *Electric vehicle technology explained* (2nd ed.). Chichester, West Sussex, UK: Wiley.
59. Levin, M. W., Duell, M., & Waller, S. T. (2014). *Effect of road grade on networkwide vehicle energy consumption and ecorouting*. Transportation Research Record: Journal of the Transportation Research Board, No. 2427, Transportation Research Board of the National Academies, Washington, pp. 26–33.
60. Lipp, T., & Boyd, S. (2014). Minimum-time speed optimisation over a fixed path. *International Journal of Control, 87*(6), 1297–1311.
61. Liu, G., Ouyang, M., Lu, L., Li, J., & Han, X. (2015). Online estimation of lithium-ion battery remaining discharge capacity through differential voltage analysis. *Journal of Power Sources, 274,* 971–989.
62. Lu, D., & Ouyang, M. (2014). Torque-based optimal acceleration control for electric vehicle. *Chinese Journal of Mechanical Engineering (English Edition), 27*(2), 319–330.

63. Mehar S., & Rémy, G. (2013). EV-planning: Electric vehicle itinerary planning. In *Proceeding of IEEE International Conference on Smart Communications in Network Technologies (SaCoNeT)*, June 17–19, 2013, Paris (pp. 1–5). https://doi.org/10.1109/saconet.2013.6654583.
64. Miettinen, K. (1999). *Nonlinear multiobjective optimization*. Boston: Kluwer.
65. Moura, A., Rijo, R., Silva, P., & Crespo, S. (2010). A multi-objective genetic algorithm applied to autonomous underwater vehicles for sewage outfall plume dispersion observations. *Applied Soft Computing, 10*(4), 1119–1126.
66. Nan, Z., & Gouzhong, M. A. (2007). Research on the theory and application of road speed limit. In *Proceedings of the first international Conference on Transportation Engineering*, Southwest Jiaotong University, Chengdu, China, July 22–24, 2007 (pp. 2699–2704).
67. Nandi, A. K., Deb, K., Ganguly, S., & Datta, S. (2012). Investigating the role of metallic fillers in particulate reinforced flexible mould material composites using evolutionary algorithms. *Applied Soft Computing, 12,* 28–39.
68. Nandi, A. K., Chakraborty, D., & Vaz, W. (2015). Design of a comfortable optimal driving strategy for electric vehicles using multi-objective optimization. *Journal of Power Sources, 283*(2015), 1–18.
69. NAVTEQ ADAS for Hyundai [NAH]. (2012). Retrieved December, 2014, from http://press.navteq.com/NAVTEQ-Map-Powers-New-Navigation-System-For-Hyundai-Solaris.
70. NRC. (2006). *Tires and passenger vehicle fuel economy—Informing consumers, improving performance*. Transportation Research Board. Washington D.C., USA: National Research Council of the National Academies (Special report 286).
71. Oduguwa, V., Tiwari, A., & Roy, R. (2005). Evolutionary computing in manufacturing industry: An overview of recent applications. *Applied Soft Computing, 5*(3), 281–299.
72. Onieva, E., Naranjo, J. E., Milanes, V., Alonso, J., Garcia, R., & Perez, J. (2011). Automatic lateral control for unmanned vehicles via genetic algorithms. *Applied Soft Computing, 11*(1), 1303–1309.
73. Orazem, M. E., & Tribollet, B. (2011). *Electrochemical impedance spectroscopy*. Wiley, Hoboken.
74. Ostensen, A. G. (1997). Effects of raising and lowering speed limits on selected roadway sections. U.S. Department of Transportation, Federal Highway Administration, Publication No. FHWA-RD-97-084.
75. Ramakers, R., Henning, K., Gies, S., Abel, D., & Max, H. (2009). Electronically coupled truck platoons on German highways. In *IEEE International Conference on Systems, Man and Cybernetics (SMC 2009)* (pp. S.2409–S.2414).
76. Sachenbacher, M., Leucker, M., Artmeier, A., & Haselmayr, J. (2011). Efficient energy-optimal routing for electric vehicles. In *Proceedings of the Twenty-Fifth AAAI Conference on Artificial Intelligence*, Hyatt Regency San Francisco, August 7–11, 2011 (pp. 1402–1407).
77. Sandro, B. (2011). ID4EV—Intelligent dynamics for fully electric vehicles Barcelona motor show. Barcelona, May 18, 2011.
78. Sengupta, A., & Upadhyay, A. (2009). Locating the critical failure surface in a slope stability analysis by genetic algorithm. *Applied Soft Computing, 9*(1), 387–392.
79. Shankar, R., & Marco, J. (2013). Method for estimating the energy consumption of electric vehicles and plug-in hybrid electric vehicles under real-world driving conditions. *IET Intelligent Transport Systems, 7*(1), 138–150.
80. Shen, W. X., Chau, K. T., Chan, C. C., & Lo, E. W. C. (2005). Neural network-based residual capacity indicator for nickel-metal hydride batteries in electric vehicles. *IEEE Transactions on Vehicular Technology, 54*(5), 1705–1712.
81. Shladover, S. (2008). AHS research at the California PATH program and future AHS research needs. In *IEEE International Conference on Vehicular Electronics and Safety (ICVES 2008)* (pp. S.4–S.5).
82. Shortt, A., & O'Malley, M. (2009). Impact of optimal charging of electric vehicles on future generation portfolios. In *Proceeding of IEEE PES/IAS Conference on Sustainable Alternative Energy (SAE)*, Valencia, Spain, September 28–30, 2009. https://doi.org/10.1109/sae.2009.5534861.

83. Smith, K. A., Rahn, C. D., & Wang, C. Y. (2010). Model-based electrochemical estimation and constraint management for pulse operation of lithium ion batteries. *IEEE Transactions on Control Systems Technology, 18*(3), 654–663.
84. Sundstrom, O., & Binding, C. (2010). Planning electric-drive vehicle charging under constrained grid conditions. In *Proceeding of 2010 International Conference on Power System Technology "POWERCON2010"*, Hangzhou, Zhejiang Province, China, October 24–28, 2010, published by IEEE (pp. 1–6).
85. Szumanowski, A., & Chang, Y. (2008). Battery management system based on battery nonlinear dynamics modeling. *IEEE Transactions on Vehicular Technology, 57*(3), 1425–1432.
86. The Freightliner Predictive Cruise Control [FPCC]. (2015). Retrieved January, 2015, from http://www.freightlinertrucks.com/Multimedia/MediaLibrary/Trucks/?AssetId=15990456-b11e-4966-a5be-c70e22cafcca.
87. Tsugawa, S. (1993). Super smart vehicle system: Future intelligent driving and the measures for the materialization. In *Proceeding of Surface Transportation: Mobility, Technology, and Society. Proceedings of the IVHS AMERICA 1993 Annual Meeting*, Washington, D.C., April 14–17, 1993 (pp 192–198).
88. Van Mierlo, J., Maggetto, G., Van De Burgwal, E., & Gense, R. (2004). Driving style and traffic measures—Influence on vehicle emissions and fuel consumption. *Proceedings of Institute of Mechanical Engineers Part D: Journal of Automobile Engineering, 218*(1), 43–50.
89. Vaz, W., Nandi, A. K., Landers, R. G., & Koylu, U. O. (2015). Electric vehicle range prediction for constant speed trip using multiobjective optimization. *Journal of Power Sources, 275,* 435–446.
90. Vaz, W., Nandi, A. K., & Koylu, U. O. (2016). A multi-objective approach to find optimal electric vehicle acceleration: simultaneous minimization of acceleration duration and energy consumption. *IEEE Transactions on Vehicular Technology, 65*(6), 4633–4644.
91. Vehicle Platooning and Automated Highways [VPAH]. (2013). Retrieved December 05, 2014, from http://www.path.berkeley.edu/PATH/Publications/Media/FactSheet/VPlatooning.pdf.
92. Veldhuizen, D. A. V., & Lamont, G. B. (1998). Evolutionary computation and convergence to a pareto front. In J. R. Koza, W. Banzhaf, K. Chellapilla, K. Deb, M. Dorigo, D. B. Fogel, M. H. Garzon, D. E. Goldberg, H. Iba, & R. Riolo (Eds.), *Genetic Programming 1998: Proceedings of the Third Annual Conference* (pp. 22–25), San Francisco, CA.
93. Venhovens, P. J. Th., Bernasch, J. H., Löwenau, J. P., Rieker, H. G., & Schraut, M. (1999). *The application of advanced vehicle navigation in BMW driver assistance systems*. SAE Technical Paper Series, 1999-01-0490.
94. Vexia's ecoNav solution [VES] (2012). Retrieved December, 2014, from http://www.vexia.es/en/econav_technology.htm.
95. Wang, Y., Jiang, J., & Mu, T. (2013). Context-aware and energy-driven route optimization for fully electric vehicles via crowdsourcing. *IEEE Transaction on Intelligent Transportation Systems, 14*(3), 1331–1345.
96. Wareham-Norfolk, K. (2011). Range limits of electric vehicles. *Engineering & Technology, 6*(3), 22–23.
97. Watkins, S., 7 Saunders, J. (1998). *A review of the wind conditions experienced by a moving vehicle*. SAE Technical Paper 981182.
98. Watkins, S., & Cooper, K. (2007). *The unsteady wind environment of road vehicles, Part Two: Effects on vehicle development and simulation of turbulence*. SAE Technical Paper 2007-01-1237.
99. Winner, H., Witte, S., Uhler, W., & Lichtenberg, B. (2006). *Adaptive cruise control system aspects and development trends*. SAE Technical Paper Series 961010.
100. Xu, G., Li, W., Xu, K., & Song, Z. (2011). An intelligent regenerative braking strategy for electric vehicles. *Energies, 4,* 1461–1477.
101. Yao, E. J., Wang, M. Y., Song, Y. Y., & Zuo, T. (2013). Estimating the cruising range of electric vehicle based on instantaneous speed and acceleration. *Applied Mechanics and Materials, 361–363,* 2104–2108.

102. Ygnace, J. L., Al-Deek, H. M, & Lavallee, P. (1990). *Vehicle navigation and route guidance technologies: Push and pull factors assessment*. Path (Program on Advanced Technology for the Highway) Research Report, Institute of Transportation Studies, University of California Berkeley, UCB-ITS-PRR-90-2.
103. Zervas, E. (2011). Impact of altitude on fuel consumption of a gasoline passenger car. *Fuel, 90,* 2340–2342.
104. Zhang, X., & Rice, J. A. (2003). Short-term travel time prediction. *Transportation Research Part C: Emerging Technologies, 11*(3–4), 187–210.
105. [Switzerland. TIK-Schriftenreihe Nr. 30, Diss ETH No. 13398, Shaker Verlag, Aachen, Germany].
106. Zlocki, A., Huang, Q., Ghaouty-El, M., Eckstein, L., & Grundmann, H. G. (2013). Intelligent functionalities for fully electric vehicles. In SAE-China and FISITA (Eds.), *Proceedings of the FISITA 2012 World Automotive Congress*. Lecture Notes in Electrical Engineering 200 (pp. 267–274). Berlin, Heidelberg: Springer.